Luleå Tekniska Universitet

Master Thesis, 30 hp

Experimental investigation of a de-icing system for wind turbine blades based on infrared radiation

Jennifer Pettersson, jenpeb-3@student.ltu.se

Sofia Sollén, sofsol-3@student.ltu.se

June 17, 2019

Abstract

Wind power is one of the fastest growing electrical energy producer all over the world and the expansions in Sweden are focused to the northern parts of the country. There are advantages, as good wind conditions and large unexploited areas, to build wind farms in the north but there are also problems. Due to long periods with cold climate, ice and snow accumulation on blades can be a safety risk, induce energy production losses and cause wear on wind turbine components.

Due to the de-icing systems that are not fulfilling the demands of being cost effective and mainly focuses on the leading edge, a new de-icing system based on infrared radiation has been investigated. Experiments with the new de-icing system has been performed in a small scale and full scale with a section of a real wind turbine blade. Parameters that were evaluated were power of heaters, distance, wavelength of radiation, surrounding temperature and de-icing time. The experiments were carried out in a climate hall in Arctic Falls facilities in Piteå.

The tests showed that the largest impact of the efficiency and de-icing time was the distance and the wavelength of the heaters. With two different combinations were tested, the combination with a shorter and longer wavelength was the most effective on 1.5 m distance. Except for the glaze ice, the different snow types did not have any significant impact of the de-icing. There was no large difference for the tests in different surrounding temperatures.

The main conclusion for the de-icing system is that it works, but not efficient enough to compete with the commercial systems today, even though it manage to de-ice the whole blade instead of just the leading edge. But this system has good potential if the heaters are developed to radiate a more even and concentrated beam that only focuses on the blade. This method is estimated to be a lower investment, but new economic calculations have to be done to further motivate the work.

Keywords: Wind power, Wind turbine, Cold climate, Ice and snow, De-icing, Infrared radiation.

Sammanfattning

Vindkraft är en av de snabbast växande elproducenterna i världen och utbredningen i Sverige sker framförallt i de nordliga länen. Fördelar, som goda vindförhållanden och stora obyggda områden, motiverar denna placering samtidigt som det finns nackdelar. Pågrund av långa perioder med kallt klimat fastnar is och snö på bladen vilket medför en säkerhetsrisk, ger produktionsförluster samt orsakar slitage på komponenter i vindturbinen.

Då avisningssystemen som finns idag inte uppfyller behoven och avisningen endast är fokuserad till framkanten av bladet, har ett nytt avisningssystem baserat på infraröd strålning blivit undersökt. Experiment med denna nya metod har utförst små- och storskaligt på en del av ett vindturbinsblad. Parametrarna som undersöktes var effekten hos värmare, avstånd, våglängd hos strålningen, omgivningens temperatur samt avisningstiden.

Testerna visade att avståndet mellan värmare och blad samt våglängden hos värmarna påverkade verkningsgraden och avisningstiden mest. Två olika kombinationer av värmare användes i testerna där kombinationen med ett bredare spektra av våglängder var mer effektiv och det på 1.5 m avstånd. Förutom för testerna med klaris var inte skillnaden mellan de olika snötyperna särskilt stor. Inte heller experiment med olika omgivningstemperatur visade någon större skillnad.

Det nya avisningssystemet fungerar, men inte tillräckligt effektivt jämfört med de system som redan finns implementerade idag. Samtidigt möjliggör detta system att en större del av bladet blir avisat, inte endast framkanten. Det finns potential för att i framtiden använda ett avisningssytem för vindkraftverk som är baserat på infraröd strålning. Men då måste värmarna utvecklas för att uppnå en mer fokuserad strålning och där med möjliggöra ett ökat avstånd mellan blad och värmare. Utifrån uppskattade värden innebär detta system en lägre investering, men nya ekonomiska beräkningar bör genomföras för att motivera ett fortsatt arbete.

Nyckelord: Vindkraft, Vindturbin, Kallt klimat, Snö och is, Avisning, Infraröd strålning.

Preface

This report is the master thesis of two students at Luleå University of technology, LTU. The master thesis is finishing the studies for *Master of Science in Sustainable Energy Engineering* with specialisation in *Wind and Hydro Power*. The master thesis is a project for Vattenfall Research and Development, R&D, at the department Rotating Machines within the Wind portfolio.

The project was carried out in the spring of 2019 for 20 weeks, from January until June. Two presentations were held in the end of the project, one at Luleå University of Technology in Luleå and one at the head office of Vattenfall AB in Solna, Stockholm.

In the beginning of the project a study visit to a wind turbine cite in Stor-Rotliden was included and later a visit to Vattenfall AB R&D research facilities in Älvkarleby. Most of the work has been performed in distance due to different locations (Luleå and Solna), but the experimental work has been performed in Luleå and Piteå in the county of Norrbotten.

Acknowledgements

There were many people involved in this project in addition to us, the two master thesis students. These people have helped us with everything from invaluable knowledge, snow making and transportation of a wind turbine blade section all the way from Denmark. This project would not have been possible in this extend without our supervisors that have supported and encouraged us to work independently.

- *Jan Ukonsaari*, supervisor, Senior R&D Engineer at Vattenfall AB, R&D at the department of Rotating Machines in Luleå.
- *Lavan Kumar Eppanapelli*, supervisor, Researcher at Luleå University of Technology at the department of Fluid and Experimental Mechanics.
- *Johan Casselgren*, supervisor and examiner, Associate Professor at Luleå University of Technology at the department of Fluid and Experimental Mechanics.

- *Pär Attermo*, founder of the idea for the project, Investment Management at Vattenfall AB, BA Wind in Solna.
- *Peter Krohn*, knowledge about wind turbines in cold climate, Senior R&D Engineer at Vattenfall AB, R&D at the department of Rotating Machines in Älvkarleby.
- *Mats and John Rousk*, support and delivery of infrared heaters, Opranic Sweden AB.
- *Per Engström*, storage and electrical support, project manager at Vattenfall Service Nordic AB in Luleå.
- *Marcus Samuelsson* and his co-workers, snow making and coffee for the breaks outside the cold climate chamber, Arctic Falls AB in Piteå.
- *Per Gren*, knowledge about radiation and supplier of equipment, Senior Lecturer at Luleå University of Technology at the department of Fluid and Experimental Mechanics.
- Our co-workers at Vattenfall AB in Solna and Luleå.
- Friends and family that have supported us all the way through our studies at the university.

Jennifer Pettersson & Sofia Sollén

Solna, Sweden June, 2019

Table of contents

List of Figures viii

List of Tables xi

List of Variables xii

1 Introduction 1
- 1.1 Vattenfall . . . 2
  - 1.1.1 Innovation contest, winning idea 2018 . . . 2
- 1.2 Objectives and purpose . . . 3
- 1.3 Scope and limitations . . . 3

2 Background 4
- 2.1 Fundamentals of wind turbines . . . 4
- 2.2 Wind turbines in cold climate . . . 6
  - 2.2.1 Ice detection and monitoring . . . 9
- 2.3 De-icing and anti-icing . . . 10
  - 2.3.1 Thermal heat elements . . . 10
  - 2.3.2 Hot air de-icing system . . . 13
- 2.4 Other applications of infrared heating for de-icing or anti-icing 14
  - 2.4.1 Airplanes . . . 14
  - 2.4.2 Public areas . . . 15

3 Theory 17
- 3.1 Ice and snow . . . 17
- 3.2 Infrared radiation . . . 19
- 3.3 Calculations . . . 20
  - 3.3.1 Heat transfer . . . 20
  - 3.3.2 Radiation . . . 22

4 Equipment 23
- 4.1 Infrared heaters . . . 23
- 4.2 Test objects . . . 25
- 4.3 Thermal camera . . . 26
- 4.4 Thermocouple . . . 27
- 4.5 Tension load cell . . . 27
- 4.6 Data acquisition . . . 28
- 4.7 Thermopile sensor . . . 29

5 Methodology **31**
5.1 Risk assessment . . . 31
5.2 Intensity of radiation . . . 32
5.2.1 Single heater, 2.6 kW . . . 32
5.2.2 Multiple heaters, 7.8 kW . . . 33
5.3 Small scale tests . . . 34
5.3.1 Glaze ice build-up . . . 34
5.3.2 Glaze ice, experimental setup . . . 35
5.3.3 Snow build-up . . . 37
5.3.4 Snow, experimental setup . . . 38
5.4 Full scale tests . . . 39
5.4.1 Snow build-up . . . 39
5.4.2 Experimental setup . . . 40
5.5 Definitions . . . 41
5.5.1 Total test time . . . 41
5.5.2 Time of de-icing . . . 42
5.5.3 Time of start sequence . . . 42
5.5.4 Melting rate . . . 42
5.5.5 Temperature gradient . . . 42
5.5.6 Efficiency . . . 43
5.6 Modeling . . . 43

6 Results **44**
6.1 Intensity of radiation . . . 44
6.1.1 Single heater, 2.6 kW . . . 44
6.1.2 Multiple heaters, 7.8 kW . . . 45
6.2 Small scale, glaze ice . . . 49
6.2.1 Test B: IR-X at 0.5 m, glaze ice . . . 50
6.2.2 Test E: Halogen at 0.5 m, glaze ice . . . 53
6.3 Small scale, snow . . . 54
6.3.1 Test F: Halogen at 0.5 m, snow -30 °C . . . 55
6.3.2 Test G: IR-X at 0.5 m, snow -30 °C . . . 55
6.3.3 Test H: IR-X at 0.5 m, snow -15 °C . . . 56
6.3.4 Test I: Halogen at 0.5 m, snow -15 °C . . . 57
6.4 Full scale tests . . . 58
6.4.1 Test 2: 3 IR-X at 1 m, dry snow . . . 59
6.4.2 Test 3: 3 IR-X at 1.5 m, dry snow . . . 61
6.4.3 Test 4: 2 IR-X & 1 Halogen at 1 m, dry snow . . . 63
6.4.4 Test 5: 2 IR-X & 1 Halogen at 1.5 m, dry snow . . . 65
6.4.5 Test 6: 2 IR-X & 1 Halogen at 1.5 m, wet snow . . . 67
6.5 Modeling . . . 69

6.5.1 Forced wind convection 70

7 Analysis **71**
7.1 Small scale tests, glaze ice 71
7.1.1 IR-X 71
7.1.2 Carbon 72
7.1.3 Halogen 72
7.2 Small scale tests, snow 73
7.3 Full scale tests 73
7.3.1 Different distances 74
7.3.2 Different combinations of heaters 74
7.3.3 Different snow types 75

8 Discussion and Conclusion **76**
8.1 Uncertainties and errors 77

9 Further Work **79**

References **80**

Appendix A - Case Study: Stor-Rotliden **I**

Appendix B - Thermal tables **III**

Appendix C - List of equipment **IV**

Appendix D - MATLAB commands **V**

Appendix E - Load cell data sheet **VI**

Appendix F - Risk assessment **VII**

Appendix G - Small scale results **VIII**

Appendix H - Full scale results **XI**

List of Figures

1 Different placings of infrared heaters. 2
2 An overview of a wind turbine with the main parts. 4
3 Definitions of angles and pitch. 5
4 The forces acting on the blade. 5
5 A sequence of ice falling from a wind turbine blade [11]. 7
6 Power curves, February. 8
7 Power curves, July. 8
8 Power curve [15]. 9
9 An overview of how the thermal electric mat is placed [16]. . . 11
10 Heating mat that is placed at the leading edge [16]. 11
11 Images of thermal heat elements as de-icing system. 12
12 A consequence of having a thermal heating system at a blade [17]. 12
13 Hot air de-icing system [19]. 13
14 De-icing of airplane with IR-heaters at JFK International Airport [24]. 15
15 Two different infrared heaters available at the market. 16
16 Type of icing depending of wind speed and air temperature [28]. 18
17 Three different types of in-cloud icing. 18
18 Ice creation on wind turbines in Stor-Rotliden, February 2019. 19
19 Electromagnetic spectra for infrared radiation [35]. 19
20 Reflectance for different materials and wavelengths [36] 20
21 Infrared heaters supplied by Opranic. 24
22 Test objects. 26
23 Thermal camera, Testo 875i. 27
24 Tension load cell. 28
25 Pinout for NI-DAQ 9219. 29
26 Thermopile sensor. 30
27 The setup for the experimental test with a thermopile sensor. 32
28 Measured points over a 2x2m surface. 33
29 Ice build-up procedure for small scale tests with glaze ice. . . . 35
30 Experimental setup for the small scale tests. 36
31 Experimental setup in the freezer. 37
32 Snow build-up for small scale tests. 38
33 Experimental setup for the small scale test with snow. 39
34 Snow build-up for the full scale tests. 40
35 Experimental setup for the full scale tests. 41
36 A block diagram of how the model is created. 43

37 Measured intensity for all the heaters, with and without shield. 45
38 Intensity distribution for heater combination with 3 IR-X. . . 46
39 Power for different distances for the heater combination with 3 IR-X. 47
40 Intensity distribution for heater combination with 2 IR-X and 1 Halogen. 48
41 Power for different distances for the combined heater with 2 IR-X and and 1 Halogen. 48
42 Temperatures measured with thermocouples for Test B,C and D. 50
43 Temperature at the surface of the ice and fiberglass plate measured with the thermal camera. 50
44 Images and heat charts in time sequences for Test B, IR-X 0.5 m, glaze ice. 52
45 Images and heat charts in time sequences for Test E, Halogen 0.5 m, glaze ice. 53
46 Average temperature measured with the thermal camera for Test f,G,H and I. 54
47 Images and heat charts in time sequences for Test F, Halogen 0.5 m, snow -30 °C. 55
48 Images and heat charts in time sequences for Test G, IR-X 0.5 m, snow -30 °C. 56
49 Images and heat charts in time sequences for Test H, IR-X 0.5 m, snow -15 °C. 57
50 Images and heat charts in time sequences for Test I, Halogen 0.5 m, snow -15 °C. 58
51 Images of full blade for Test 2. 59
52 Images of snow on the edges for Test 2. 60
53 Weight of snow (blue) and maximal average temperature at the surface (red) for Test 2. 60
54 Images of full blade for Test 3. 61
55 Images of snow on the edges for Test 3. 62
56 Weight of snow (blue) and maximal average temperature at the surface (red) for Test 3. 62
57 Images of full blade for Test 4. 63
58 Images of snow on the edges for Test 4. 64
59 Weight of snow (blue) and maximal average temperature at the surface (red) for Test 4. 64
60 Images of full blade for Test 4. 65
61 Images of snow on the edges for Test 5. 66

62 Weight of snow (blue) and maximal average temperature at the surface (red) for Test 5. 66
63 Images of full blade for Test 6. 67
64 Images of snow on the edges for Test 6. 68
65 Weight of snow (blue) and maximal average temperature at the surface (red) for Test 6. 68
66 De-icing time in min/kg for different distances (1-5 m) for the two combination of heaters. 69
67 De-icing time with convection considered for the two combination of heaters. 70
68 Flowchart of how to determine the losses. I
69 Bar graph for the distribution of losses and the expected power. II
70 Images and heat charts for Test A, IR-X 1 m, glaze ice. VIII
71 Images and heat charts for Test C, Halogen 0.5 m, glaze ice. . IX
72 Images and heat charts for Test D, Carbon 0.5 m, glaze ice. . X
73 Images of full blade for Test 1. XI
74 Images of snow on the edges for Test 1. XII
75 Weight and temperature graph for Test 1. XII
76 Images of full blade for Test 7. XIII
77 Images of snow on the edges for Test 7. XIV
78 Weight and temperature graph for test 7. XIV
79 Images of full blade for Test 8. XV
80 Images of snow on the edges for Test 8. XVI
81 Weight and temperature graph for Test 8. XVI

List of Tables

1 Properties of atmospheric icing [28]. 17
2 List of equipment. 23
3 Specifications of the different heaters. 25
4 Cable colors for the load cell, VZ101BH. 28
5 Signals by mode for NI-DAQ 9219. 29
6 Signal description for NI-DAQ 9219. 29
7 Test matrix for the different points for different distances, X marks a measured point. 34
8 Values from the intensity measurements for the heaters. 44
9 Measured values for the intensity for the heater combination with three IR-X. 45
10 Measured intensity values for the combined heaters. 47
11 Comparison of infrared heaters with a power of 2.6 kW for glaze ice. 49
12 Comparison of infrared heaters with a power of 2.6 kW for snow. 54
13 All the full scale tests summarised in one table. 59
14 Prandtl number. III

List of Variables

Sign	Unit	Variable
A	m^2	Area
b	-	Constant of proportionality
c_p	J/kgK	Specific heat capacity
I	W/m^2	Intensity
f	Hz	Frequency
L_f	J/kg	Latent heat of fusion
m	kg	Mass
P	W	Power
Q	J	Energy
T	$K,^\circ C$	Temperature
V	m/s	Wind speed
ϵ	-	Emissivity
ρ	kg/m^3	Density
σ	J/m^2sK^4	Constant of Stefan-Boltzmann
λ	m	Wavelength

1 Introduction

The energy and climate topic has never been as important and relevant as today. Renewable energy sources are increasing and large investments are disposed to research [1]. Wind power is one of the fastest growing electrical energy producer all over the world [2] which also includes Sweden.

The Swedish government has set goals that at least 50 % of Sweden's energy use should come from renewable energy resources by 2020 [3] and for this, wind power is going to have an important role. With the wind power expanding all over the country, Vattenfall AB is investing in 84 new wind turbines until 2022 with focus in the northern parts of Sweden [4].

The northern parts of Sweden has a lot of potential for wind power due to good wind conditions and large unexploited areas where it is advantageously to build large farms. But in the north there are also problems that follows with the cold climate and the long winters. In a cold climate the wind turbines are more exposed to snow and ice accumulation on the blades [1]. Snow and ice build-up on blades can be a safety risk, induce energy production losses and can also cause wear on the wind turbine components. The energy loss due to icing can be up to 20 % of the annual production [5][6].

For these problems there are a few techniques used as de-icing systems today. The two most common systems includes thermal heat elements in the surface of the blade or blowing hot air inside the blade. These techniques requires a significant amount of power and are mostly focused on the leading edge of the blade. In harsh climate conditions the techniques has showed to be inefficient.

In this master thesis a new de-icing system will be investigated and tested. The technique of the system is based on infrared radiation and the idea is to implement heaters to melt ice and snow on the blades. This is investigated by performing experimental tests to confirm the efficiency of the method. The experimental tests will include small scale tests on fibreglass plates similar to the surface of a wind turbine blade. Full scale tests on a section of a real wind turbine blade will also be performed to validate the results. The experiments will be performed by varying different parameters as snow type, distance and wavelength of the radiation. Theoretical studies will also be performed which includes thermal heat transfer, radiation and modeling in the software MATLAB.

1.1 Vattenfall

Vattenfall AB is an energy company owned by the Swedish government with 20 000 employees. Their main markets are Sweden, Germany, Netherlands, Denmark and the United Kingdom. Vattenfall R&D is a subdivision of Vattenfall and has approximately 130 employees that are working with new technology in different areas. Rotating Machines are conducting the research in rotating machinery and mechanical structure related to hydro power and wind power for Vattenfall.

Every year Vattenfall has an internal innovation contest to encourage their employees to develop new innovations to make way for a world without fossil fuels. At the contest of 2018, Pär Attermo applied and won the contest with the idea of a new de-icing system for wind turbines that is the start of this master thesis.

1.1.1 Innovation contest, winning idea 2018

The concept of the winning idea can be seen in Figure 1. The system could be mounted at the tower or at a swing arm to reach further out. The turbine is intended to stop for each blade parallel to the tower and de-ice one blade at a time. From estimated values this new de-icing system should be more efficient and result in a lower investment than the de-icing systems of today.

(a) Placing on the tower.

(b) Placing on a swing arm.

Figure 1: Different placings of infrared heaters.

1.2 Objectives and purpose

To investigate this new de-icing system there are some aspects that are important to include. The technique of melting ice and snow on a fiberglass surface has to be tested and proven effective. The efficiency of the technique has to be evaluated and the main parameters to study are:

- Wavelength and material of heater.
- Power of the heater.
- Optimal distance between heater and blade.
- Surrounding temperature.
- Time of the de-icing sequence.
- Achievability.

The purpose of this project is to do a feasibility study to determine if this de-icing method with infrared heating is applicable on wind turbine blades. A de-icing model based on the parameters above will determine the dimensions of the infrared de-icing system and give recommendations for future work. This because the commercial systems today are not efficient enough on severe ice accumulation.

1.3 Scope and limitations

The work will include theoretical calculations for the thermal heat transfer and also include experimental tests of the de-icing system. The testing will start in a small scale and then be upgraded to perform full scale tests to verify the results. Field tests on site at an existing wind turbine will not be conducted in this project due to lack of time and finances. This feasibility study needs to be done to motivate an eventual larger investment.

The mechanical and electrical design will not be investigated or in focus for this thesis though it will be considered for the future work and design of the system. Application of ice detection and anti-icing in combination with the de-icing system will not be included in the project due to limitation of time. Furthermore an economical analysis is not included.

2 Background

In the following chapter the background of the project is described. The problems with wind power in cold climate are introduced together with information about already existing de-icing systems for wind turbines. Other applications of infrared, IR, de-icing systems are also presented.

2.1 Fundamentals of wind turbines

A wind turbine has four fundamental parts, foundation, nacelle, tower and blades, see Figure 2a. The nacelle includes main parts as generator, gearbox, bearings and shafts as seen in Figure 2b. The material of the turbine blades is usually fiberglass and epoxy with a core of wood or similar. For protection against erosion and wear the surface of the blades are usually covered with a hard wearing top coating.

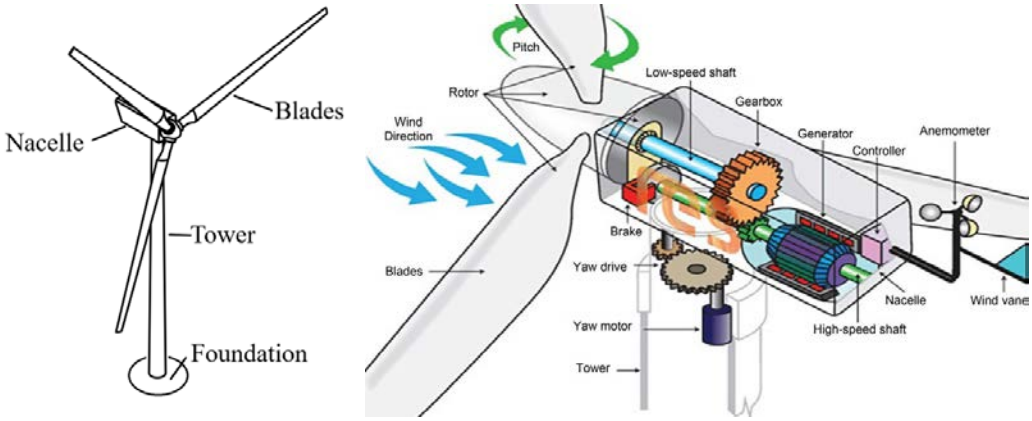

(a) Fundamental parts. (b) Components in the nacelle [7].

Figure 2: An overview of a wind turbine with the main parts.

The basic principle of how a wind turbine works is that energy from the wind is generating the rotor to spin, converting it into kinetic energy. For most of the commercial wind turbines the rotor is connected to a gearbox by shaft, converting the low speed from the rotor into high speed for the generator. With the high speed in the generator, a magnetic field is created and the energy is transformed into electricity. There are also wind turbines that are directly connected to the generator without a gearbox [8].

What initiates the rotor to spin is in first hand that the turbine has to be positioned correctly against the wind. The angle between the wind direction and the chord line of the blade is called angle of attack α, seen in Figure 3.

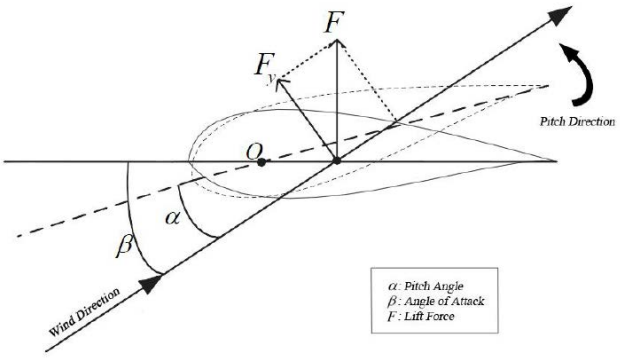

Figure 3: Definitions of angles and pitch.

The velocity increases with the radius of the sweep area which is why blades are designed with a twist and different airfoil profiles to obtain an aerodynamic design. The aerodynamics of the blades optimises the efficiency. The airflow is desired to follow the surface of the blade well to create a high and low pressure side of the blade. The pressure difference on the blade is called lift force and is the same type of force acting on the wings of an airplane, see Figure 4. The lift force is always perpendicular to the wind direction. Another force is drag force which is in the direction of the wind. These two forces are optimised from the angle of attack to improve the efficiency [8].

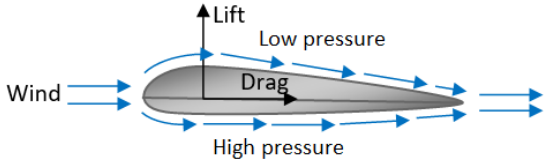

Figure 4: The forces acting on the blade.

In today's modern technology a method called pitch has been developed. Pitch is the method to control the angle of attack for the wind turbine blades.

To change the angle of attack, the blades are pitched by increasing or decreasing the blade angle, also known as pitch angle. When the wind speed is changing, the blades are pitched to obtain the best angle of attack and increase and control the power output. The correlation between the angles can be seen in Figure 3.

Another technique, used to catch the wind is the yaw control. The yaw control is a system that rotates the whole nacelle to angle or position the rotor in the direction of the wind.

2.2 Wind turbines in cold climate

Ice and snow accumulation on wind turbine blades is a significant problem in various aspects. The main aspects are listed below:

- Safety.
- Production losses.
- Wear and damage (maintenance).

The safety aspect is mainly due to the risk of ice throw or ice falling off the blades. Ice falling from a height, like a wind turbine, hits the ground with a high force. Even worse is when large or small pieces of ice are thrown from the blades when the turbine is rotating. The speed of the ice can reach a high velocity if it is thrown from the tip of the blade and may cause damage of the surroundings [9].

When there is a high risk of ice throw in the wind park the maintenance workers are recommended to not enter the area due to safety. This causes problems for the maintenance when for example a turbine stops and needs to manually be restarted at site. The severe ice throw has sometimes led to the stairs for entering the tower has been totally destroyed due to the force of the ice at high velocities [10]. A sequence of ice falling from a wind turbine blade is shown in Figure 5.

Figure 5: A sequence of ice falling from a wind turbine blade [11].

Beside the safety aspects the ice accumulation negatively affects the production. The losses caused by operations in cold climate can be up to 20 % for a full year production [5][6]. An example of the losses in production can be seen in a case study for Stor-Rotliden in Appendix A. The losses can be divided into two different types, production losses and standstill losses. Production losses occurs due to ice and snow that accumulates on the surface of the blade and changing the aerodynamic properties. If for example ice is built-up on the leading edge of the blade, the wind flow that is desired to follow the blade is going to take another path. This implies that the air flow separates from the surface and vortexes will occur and cause the lift force to decrease, which means that there will be losses. Standstill losses is the losses due to the heavy ice that has formed on the blades obstructs the turbine to operate, and therefor the turbine has to stand still.

In the north part of Sweden, Vattenfall AB has two wind power sites called Stor-Rotliden and Juktan. Stor-Rotliden have 40 turbines and an installed capacity of 78 MW. Although it is located in the north, there is no de-icing system installed. Juktan have 9 turbines and an installed capacity of 29 MW [12][13]. The turbines in Juktan have a de-icing system installed with the technique of thermal heating elements.

Power curves for Stor-Rotliden and Juktan, see Figure 6a and 6b shows the active power produced, on the y-axis, for a certain wind speed, on the x-axis. The active power is both produced and consumed power including the de-icing system. In Figure 6a a lot of losses can be seen in form of deviations. These losses are most likely due to ice and snow on the wind turbine blades. In comparison to the power curve for Juktan, Figure 6b that has a de-icing system, the losses are higher and the importance of having a de-icing system

is visualised.

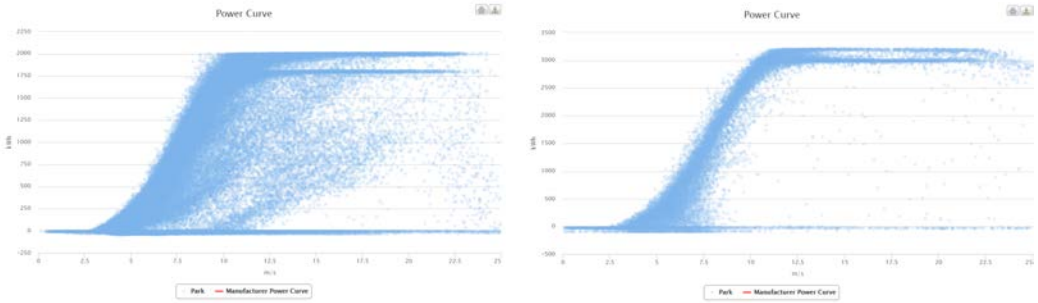

(a) Power curve for Stor-Rotliden from February, 2019.

(b) Power curve for Juktan from February, 2019

Figure 6: Power curves, February.

For the same wind farms, power curves from summer time are shown in Figure 7a and 7b. Compared to the power curves, see Figure 6a and 6b, there are less deviations and losses.

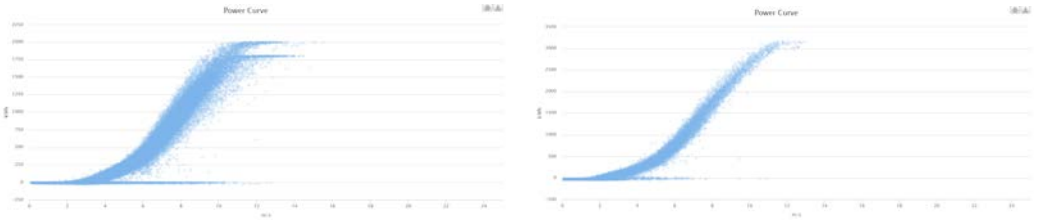

(a) Power curve for Stor-Rotliden from July, 2018.

(b) Power curve for Juktan from July, 2018

Figure 7: Power curves, July.

Another problem with the added weight on the blades is that it may cause the rotor to be unbalanced. If the rotor is unbalanced it can lead to wear and damage in bearings and the gearbox. This can cause unnecessarily expenses if parts in the turbine needs to be changed before they have served their expected lifetime [9].

The icing on turbine blades also creates a different noise. Thus the ice accumulation changes the aerodynamic profile of the blade this also initiates to change the acoustics of the turbine. This generates more noise and increase the sound level which is a regulation that is important to follow [9].

There are some existing de-icing methods that are used today and a lot of research is on going right now. Some of them are already implemented as heating elements and the hot air system. The approach of de-icing systems are different for most of the methods. For example there are coatings, anti-icing systems that experiments with paint and ultrasonic vibration methods. Coatings are often focused to be designed to be super-hydrophobic so the snow does not attach to the blade in first hand. There has been some more or less successive ideas but nothing that is working good enough on severe icing [14].

2.2.1 Ice detection and monitoring

In order to de-ice a wind turbine blade it first has to be detected. The most common method to do this is by analysing power curves. A power curve is a curve containing information about how much active power in relation to the wind speed that are produced. If larger losses are identified during operation in cold climate, assumptions are made that there is ice and snow build-up on the blade. The losses in the production is automatised to be identified in the control system. When the losses is large enough, approximately 20 %, the control system decides if the turbine should start to de-ice or just stop, depending if the turbine has a de-icing system.

An example of a power curve can be seen in Figure 8. The scattered points gives an estimation of how the production data is weighted against the manufacturer curve.

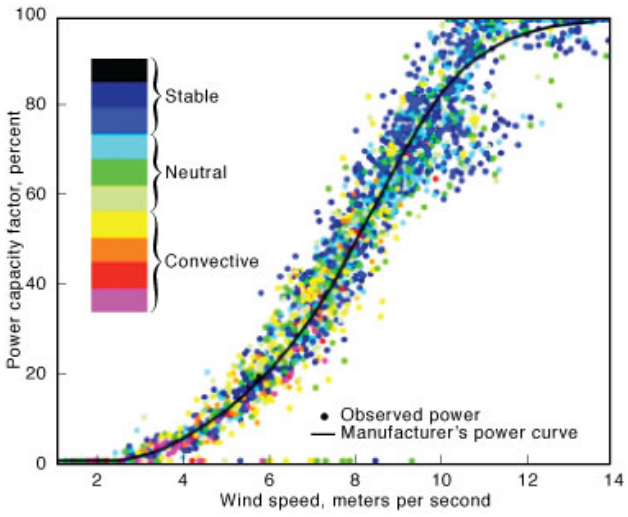

Figure 8: Power curve [15].

Although this method of analysing is quite implemented, it does not fulfill the requirement good enough. There are still problems to regulate the de-icing time, how long time it is needed to de-ice the blades sufficiently. Another problem can be to plan the de-icing after the weather conditions and have a more efficient de-icing sequence.

Other types of identifying ice are by measuring the natural frequency, visual inspections and ice sensors measuring the ice accumulation [9]. One research project that is on-going at Vattenfall R&D is to detect icing with image analysis.

2.3 De-icing and anti-icing

In this section, the two most common de-icing techniques are presented, thermal heat elements and the hot air de-icing system.

A de-icing system is often designed to melt the ice after it already has been accumulated. The purpose of an anti-icing system is to prevent the ice to accumulate in first hand. The de-icing system is used when the turbine is in non-operational mode. An anti-icing system can be divided into two different types, passive and active. A passive system can be systems that is based on coatings or paint while an active system is often thermal heat systems that can be active during operation [14].

2.3.1 Thermal heat elements

One of the most common de-icing system used as a commercial product is the thermal heat element system. The systems technique is to heat the blade from the inside and out by applying current through a carbon-fibre heating mat. The mat is built-in underneath the blade surface at the manufacturer [16]. The carbon-fibre is usually placed one layer under the top coat as seen in Figure 9, note that the scales are not necessary proportional.

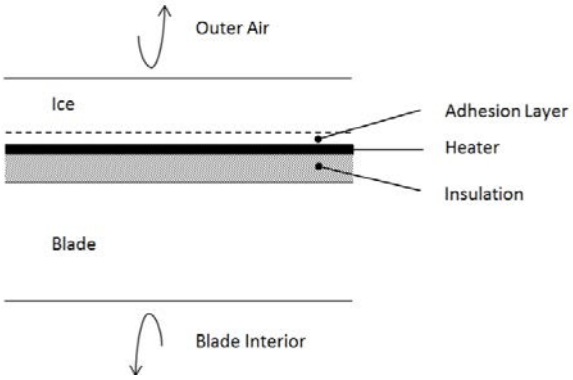

Figure 9: An overview of how the thermal electric mat is placed [16].

The method can be used as both a de-icing and anti-icing system. Which means it can both be used in non-operational mode and in operational mode. The elements are most often focused to heat only the leading edge, which is the most exposed area. It is also common that the elements are placed on the outer part of the blade where the losses is higher due to a larger sweep area. [14]. One suggestion of how heating elements are used can be seen in Figure 10.

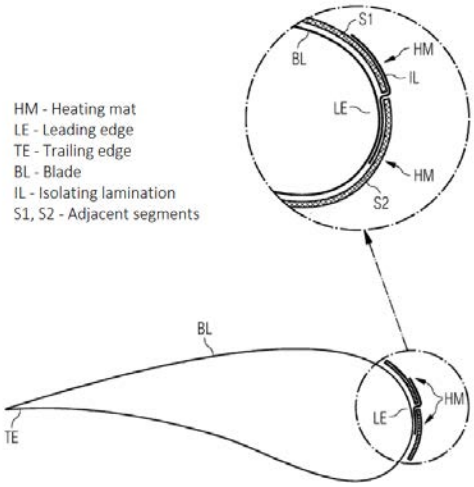

Figure 10: Heating mat that is placed at the leading edge [16].

The method has been proved to be quite efficient with quite low energy output, but still has some problems.

When the ice is melting on the blade it turns to water. A common problem with this water is that it freezes again when it flows and reaches a colder

area of the blade where there is no heating [14]. This is one of the problems of having a de-icing system that only focuses on the leading edge. In Figure 11a and Figure 11b a de-iced blade with thermal heat elements are shown. The images are clearly establishing the fact that the de-icing system is not effective enough to de-ice the whole blade to be categorised as de-iced.

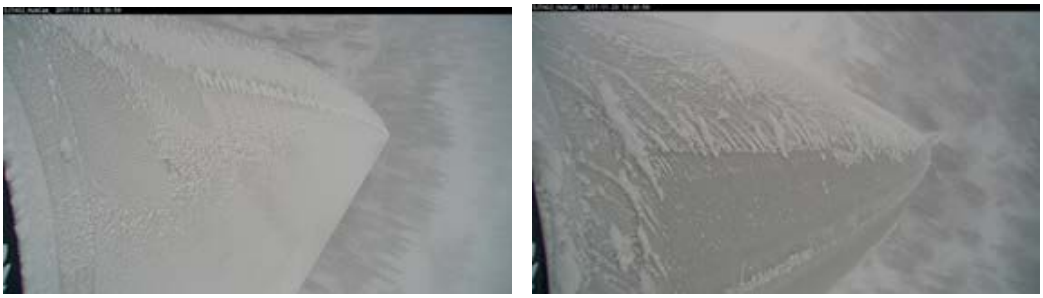

(a) Blade with ice. (b) De-iced blade.

Figure 11: Images of thermal heat elements as de-icing system.

This type of method also have problems with hot spots, which is concentrated heating that burns through the top layer of the blade and leaves a mark. In worst case a large hole is caused by the heat. In Figure 12 a severe hot spot has burnt a hole in the blade.

Figure 12: A consequence of having a thermal heating system at a blade [17].

Because the carbon fibre mat is designed to lead current it is an extra risk of damage if it is struck by lightning [14].

2.3.2 Hot air de-icing system

Another commercial and well known system is the hot air de-icing system. The system consist of three main parts: heater, fan and duct system, see Figure 13. This system can be used for anti-icing or de-icing. For the anti-icing the blade temperature is kept above zero while the de-icing is periodic where the system is in standby when no ice has occurred [18]. The system does not affect the aerodynamics of the blade or the lightening protection due to the inside placing [14].

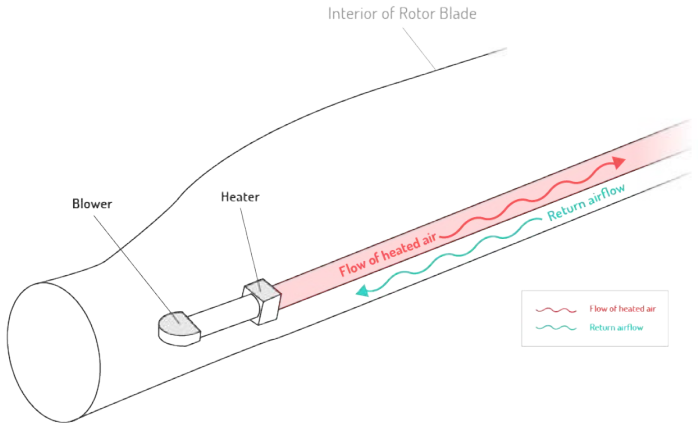

Figure 13: Hot air de-icing system [19].

Hot air is blown straight down to the tip of the blade and then circulated back to the root. The heating is focused to the tip of the blade due to highest affect of icing. There are several manufactures of this type of system and their products are similar but the largest difference between them are where they are focusing the heat. The company Vestas is only heating the outer part of the blade and the leading edge for most of the blade [20].

Enercon is another company using the same principles for de-icing. But they are heating the whole leading edge starting at the root of the blade and ending at the tip were the air is recirculated back in the mid section [21].

The de-icing time is 30-90 minutes, according to Borealis Wind, and the system can be installed on site in existing wind turbines [22][19]. But nowadays it is more common that the manufactures deliver the blades with the heating system already installed due to knowledge about the amplitude of icing at

cold climate sites.

Wind turbine blades are mostly made of fiberglass that also can be used for isolation due to lack of heat transfer. This lowers the thermal efficiency of a hot air de-icing system due to higher demand of power supply. Differing thickness along the blade also affect the heat transfer through the walls and studies made by an independent scientist shows that this system is ineffective and need more improvements to be effective [18]. Another disadvantage is the fact that the heater is placed at the root of the blade, when the heating is mostly needed at the tip, so there will be losses in the duct system due to the length of the blade [14].

2.4 Other applications of infrared heating for de-icing or anti-icing

Beside wind turbine icing there are several other industries and public areas that suffer of icing. The solutions for the problems varies and some examples of using infrared heating as a de-icing or anti-icing system will be described here.

2.4.1 Airplanes

Airplanes are in some aspects designed in a similar way as a wind turbine. It uses the wings and the aerodynamic of the wings to initiate lift power. The wings of the blade is for both an airplane and a wind turbine a really important part that is both exposed to snow and ice accumulation in cold climate.

Due to the importance of the wings, a several de-icing methods has been invented. In the same way as for wind turbines thermal heating elements are used at the leading edge of the wings to de-ice them. Other methods are to circulate hot oil and hot air, also similar to the system used for wind turbines, extracted from the engine. There are also methods that are mostly chemical-based solutions [23]. This solution is sprayed on the wings to de-ice them and prevent moist air to accumulate on the wings and other important sections on the airplane. The most common chemical used for this is glycol of different types. But in today's awareness of the environment and climate challenge, the industry is striving to avoid chemicals that is pollutant. One

of the methods that are considered to be more environmental-friendly and energy efficient is the method of using IR-radiation.

The method of using IR-radiation has been tested at several airports, including JFK International Airport in New York. The technique of heating from IR-radiation is used in a large hangar with open ends where IR-heaters are placed in the ceiling, see Figure 14. The IR-heaters are directed to spread the radiation on the airplane to de-ice it.

Figure 14: De-icing of airplane with IR-heaters at JFK International Airport [24].

De-icing with IR has been proved to be both time-effective and also cost-effective. The time for de-icing a Boeing 737 is approximately 17 minutes from when the plane enters the hangar until it leaves. This compared to the method of using glycol as de-icing that can take from 45 to 90 minutes is very effective [24]. Tests have shown that the glycol usage can be reduced by up to 90 % [24].

2.4.2 Public areas

In some public areas that is in need of de-icing, infrared radiation can be used. In Japan there is a product for de-icing public areas like parking lots and side walks with far infrared radiation. It is called Tokerumo and contains four 1 kW halogen filaments with a ceramic coating, see Figure 15a. The product is in functionality and appearance of a regular infrared heater in a larger scale and is optimal for an area of 10 m^2 according to the manufacturer [25].

There are some infrared heaters on the market in the USA where the manufacturer mention that the heater can be used for de-icing public areas. For

example the Mul-T-Mount Electric Infrared Heater from Fostoria Industries is specified with the property of controlling snow and ice [26]. This infrared heater is shown in Figure 15b and the heater comes with two or three elements of quartz that generates far infrared radiation with a power up to 10.95 kW. The reflectors are made of gold anodized aluminium and in the product sheet it is stated that the heating required for ice and snow control is in average 850 - 1110 W/m^2 [27].

(a) Drawing of the Tokerumo infrared de-icing system [25].

(b) Picture of the Mul-T-Mount Electric Infrared Heater for de-icing [26].

Figure 15: Two different infrared heaters available at the market.

Both heaters that are introduced in this section can be used in combination with more than one heater depending on the size of the target area. For the de-icing the heaters are switched on based on need, but they can also be used for anti-icing and then constant be switched on to maintain an ice-free zone as long as the temperature is below 0 °C.

3 Theory

This chapter describes the theory of ice creation and appearance, see Section 3.1, and in Section 3.2 the fundamentals of infrared radiation is presented. For calculations and simulations the theory of heat transfer and equations of radiation are included in Section 3.3.

3.1 Ice and snow

Icing of wind turbines are formed when water particles in the air collide with wind turbine blades. There are several types of snow and ice that are forming due to precipitation or in-cloud icing. For the precipitation it includes freezing rain and wet snow while in-cloud icing are glaze ice, hard rime ice or soft rime ice [28]. Different types of icing have different accretion rate depending of typical properties that is shown in Table 1. The duration is the time of the ice creation, it gives how quickly the different types of ice are forming.

The adhesion of the ice describes how strong the inter molecular forces are between the ice and the blade [29]. As an example adhesion for glaze is stronger than for soft rime where the forces can be really low. For the cohesion it is stated in the same column as adhesion in Table 1 even if they are two different properties, an assumption can be made, that the forces varies in the same way depending of the type of ice. Cohesion is the inter molecular forces between molecules with similar properties, it describes how strong the ice is internal [30].

Table 1: Properties of atmospheric icing [28].

Type of Ice	**Density [kg/m^3]**	**Adhesion & Cohesion**	**General Appearance**
Glaze	900	Strong	Transparent
Wet snow	300 - 600	Weak (forming) Strong (frozen)	White
Hard rime	600 - 900	Strong	Opaque
Soft rime	200 - 600	Low to medium	White

Type of Ice	**Droplet size**	**Humidity**	**Duration**
Glaze	Medium to large	Medium to high	Hours
Wet snow	Flakes	Very high	Hours
Hard rime	Medium	Medium	Days
Soft rime	Small	Low	Days

In Figure 16 the relation between wind speed and temperature of the surroundings indicates what type of icing that can be expected. Due to the height of the wind turbines and the large sweep area for the blades the wind speeds are high. This correlation between speed and temperature can be used for ice detection.

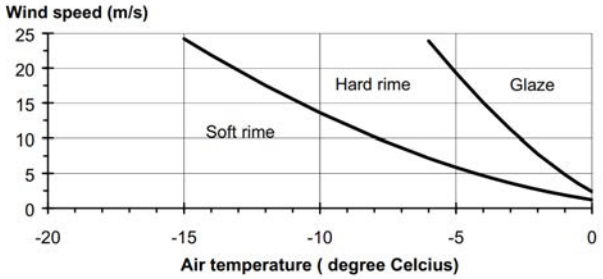

Figure 16: Type of icing depending of wind speed and air temperature [28].

The difference in appearance between rime ice and glaze ice are shown in Figure 17. Soft rime ice has a spiky and porous structure that correlate to the low density while glaze ice is solid with higher density and a clear vitreous shape. The spikes of rime points in the wind direction and the difference between soft and hard rime are distinguish, hard rime are more compact and thereby more similar to glaze ice.

(a) Soft rime ice [31]. (b) Hard rime ice [32]. (c) Glaze ice [33].

Figure 17: Three different types of in-cloud icing.

Ice accumulation on wind turbine blades in Stor-Rotliden is shown in Figure 18. The picture to the right is from a camera placed at one of the turbines to enable real time images of the current icing conditions at site. The type of icing that is shown below is from February, 2019, and appears to be rime ice due to a long period with low temperatures. At this period of time there was a large risk for ice throw and thereby a safety risk to visit the site without precautions.

Figure 18: Ice creation on wind turbines in Stor-Rotliden, February 2019.

3.2 Infrared radiation

Infrared radiation is in the electromagnetic spectra and is most commonly known as heat. The wavelength for infrared radiation is between 700 nm to 1000 μm and is outside the spectra for visible light. The spectra can be separated into different types of infrared radiation. The categories is near-, short-, mid-, long- and far-infrared where the wavelength increases with the categories, but are for Figure 19 divided into three main categories. The different types of infrared, IR, is used to different things. For example, a short-IR is used for transfer of information as in remote controls [34].

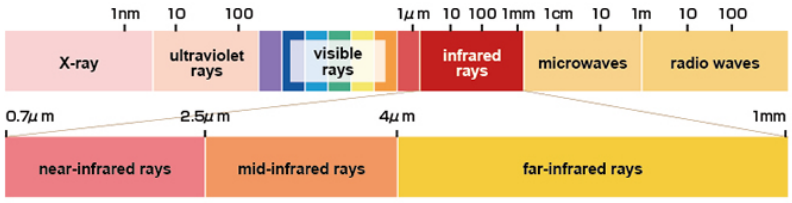

Figure 19: Electromagnetic spectra for infrared radiation [35].

.

One of the significance's of IR-heat is that it only heats the objects and not the air that is surrounding the object. The best surface to absorb infrared radiation is a matt and dark surface. Depending on material and emissivity the wavelength is absorbed differently.

The snow is acting almost like a black body when the wavelength is higher than 1550 nm. Which means it is a low reflectance and a high absorption of the radiation is accomplished.

Figure 20 shows the reflectance for snow and other materials for different wavelengths. For the snow is a longer wavelength desirable though it has a lower reflectance, which means a higher absorption rate.

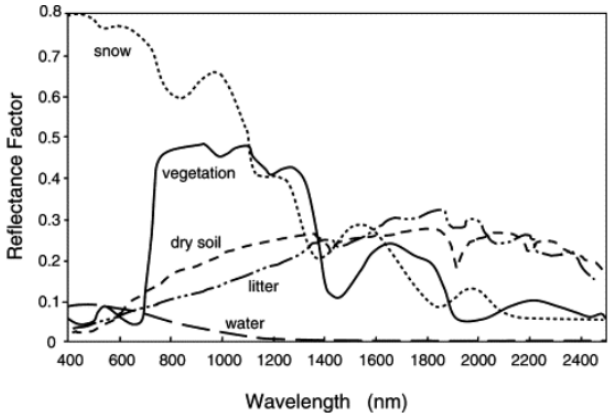

Figure 20: Reflectance for different materials and wavelengths [36]

.

3.3 Calculations

In this section, equations used in the project are presented. The equations including heat transfer, radiation and some definitions from the results. In Appendix B thermal tables can be seen.

The melting rate is defined as the mass of snow melted divided with the de-icing time, m/t_{melt}, which gives a value in kg/min. This gives an estimation of have efficient the de-icing is.

3.3.1 Heat transfer

Energy to melt the ice and snow can be calculated as the energy it takes to increase the temperature to 0 °C and the energy to melt the ice (latent heat).

The required energy to heat a material is determined by Equation 1. Where c_p is the heat capacity and ΔT is the difference between $T_0 = 0°\text{C}$ and $T_{surface}$ which is the temperature of the ice/snow surface.

$$Q_{heat} = mc_p\Delta T. \tag{1}$$

The equation to determine the latent heat, where L_f is the specific latent heat and m is the mass of the ice/snow is Equation 2

$$Q_{latent} = mL_f. \tag{2}$$

Equation 1 and 2 gives the total energy required to melt the ice.

$$Q_{melt} = Q_{heat} + Q_{latent}. \tag{3}$$

The de-icing power can then be calculated from the de-icing time as

$$P_{melt} = \frac{Q_{melt}}{t_{melt}}. \tag{4}$$

The cooling effect on the blade is calculated as forced convection and the natural convection transferred from the blade.

The natural convection is determined from Equation

$$.Q_{nat,conv} = h_c A \Delta T. \tag{5}$$

Where h_c is the convective heat transfer coefficient. For an air flow the coefficient can be approximated with Equation 6 [37].

$$h_c = 10.45 - V + 10\sqrt{V}. \tag{6}$$

For forced convection, same equation as Equation 5 is used

$$Q_{forced,conv} = hA\Delta T. \tag{7}$$

Where the convective heat transfer coefficient is determined by Nusselt number in Equation 8.

$$Nu = \frac{hL}{k}. \tag{8}$$

Where L is the characteristic length and k is the thermal conductivity.

In order to determine the Nusselt number, the Reynolds number and the Prandtl number has to be determined. Reynolds number is calculated as Equation 9.

$$Re = \frac{\rho V L}{\mu}. \tag{9}$$

From interpolation of the Prandtl number in Table 14 in Appendix B a relation for the Nusselt number, Reynolds number and Prandtl number can

be determined dependent of the size of Reynolds number in Equation 10 and 11.

$For Re < 500000$

$$Nu = 0.664 Re^{0.5} Pr^{0.33}. \tag{10}$$

$For Re > 500000$

$$Nu = Pr^{0.33}(0.037 Re^{0.8} - 871). \tag{11}$$

The heat transferred through convection is determined as the sum of Equation 5 and Equation 7.

$$Q_{convection} = Q_{nat,conv} + Q_{forced,conv}. \tag{12}$$

The measured values from the thermopile sensor is used to determine the total power on the surface (2x2 m), with bilinear interpolation. This gives the total power radiated on the surface for different distances, $P_{rad,d}$ where d is the distance.

From the radiated power and the power required for the melting, an efficiency, η_{melt} can be determined in Equation 13.

$$\eta_{melt} = \frac{P_{melt}}{P_{rad,d}}. \tag{13}$$

3.3.2 Radiation

Wavelength and temperature correlates as according to Wien's displacement law.

$$\lambda_{peak} T = 2.898 \cdot 10^{-3} mK. \tag{14}$$

For a gray body Stefan-Boltzmann's equation can be used.

$$Q_{radiation} = \varepsilon \sigma A (T_h^4 - T_c^4). \tag{15}$$

Where σ is the constant of Stefan-Boltzmann, $\sigma = 5.67 \cdot 10^{-8} J/m^2 \cdot s \cdot K^4$, and ε is emissivity and are for two bodies calculated as

$$\varepsilon = \phi_{12} \varepsilon_1 \varepsilon_2. \tag{16}$$

Even though the radiation has a high energy, the irradiance, or commonly known intensity, is important as well. The intensity is the power distribution per area and is defined as $[W/m^2]$.

$$I = \frac{P}{A}. \tag{17}$$

"The energy twice as far from the source is spread over four times the area, hence one-fourth the intensity."

4 Equipment

All equipment used for the different experimental setups can be seen in Appendix C. The more significant equipment, see Table 2, are presented in detail in this chapter. For numerical calculations MATLAB have been used as a tool, some of the built-in commands that have been implemented are included in Appendix D.

Table 2: List of equipment.

Equipment	**Manufacturers**	**Specification**
Infrared heaters	OPRANIC SWEDEN AB	IR-X, Halogen, Carbon.
Test object, plates	Unknown	1.5 x 0.5 m.
Test object, blade	Unknown	2.0 x 1.2 m, 87 kg.
Thermal camera	Testo SE & Co. KGaA	Testo 875i.
Thermocouple	Pentronic AB	Type K, –15 to 105 °C.
Tension load cell	Anyload Weigh & Measure Inc.	VZ101BH, 300 kg.
Data acquisition	National Instrument	NI-DAQ 9219.
Thermopile sensor	Ophir Optronics Solutions Ltd	10 A. NOVA II.

4.1 Infrared heaters

An infrared heater is like a lamp but with higher energy. Heat is light with a longer wavelength and light is photons that are emitted from the source when it reached a higher energy level and then fall backs to the original level. An IR-heater is in general existing of a tube filled with some type halogen gas that is highly reactive. Current is then led through the gas which makes the molecules move very fast and excite to a higher energy level to emit in form of a certain wavelength in the infrared spectra [38].

The infrared heaters that are used in this project consists of three different heaters with different materials. These heaters are investigated and tested to evaluate which material and wavelength that is best for the application of melting ice and snow on wind turbine blades.

The testes heaters are here called: Carbon, IR-X and Halogen, see Figure 21a. In Figure 21b the heaters is placed vertical in a frame. A graph of the spectra for some of the different heaters is shown in Figure 21c. The figure shows the spectra for water, for the IR-X heater and for the Halogen heater.

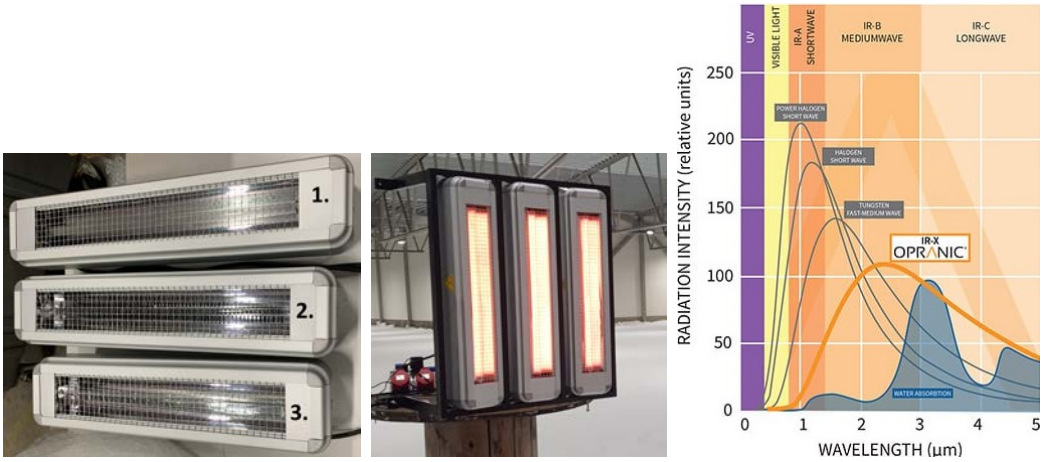

(a) The different infrared heaters by number: Carbon (1), IR-X (2) and Halogen (3).

(b) The infrared heaters placed in a frame.

(c) Graph of wavelengths for different heaters and radiation intensity [39].

Figure 21: Infrared heaters supplied by Opranic.

The heater called Halogen is a straight-forward halogen lamp. The heater has a tube that is containing halogen gas which is commonly consisting of iodine or bromine. The filament is made of Tungsten and have an emissivity value of $\varepsilon = 0.3$. The wavelength peak is about 1.4 μm and reaches a maximum temperature that is around +2000 °C. Halogen is not very absorbent for water, see Figure 21c.

The heater has a high temperature both at the elements and the output temperature. The heater also have a shorter life service than the other two heaters. Because it has a shorter wavelength, a part of the spectral range is in the visible light spectral. This means it will be a lot of visible light as well, and almost looks like a very bright regular halogen lamp.

For the Carbon heater, the elements are made of carbon fiber. The emissivity is $\varepsilon = 0.77$ and has a wavelength peak with a value about $\lambda_{peak} = 2.0\mu m$. The heater have a longer service life than Halogen. It also have a lower temperature at the element, about 1200-1300 °C. The radiant heat is softer and not as intense as the Halogen. The Carbon heater has a better absorption for water because of the longer wavelength.

IR-X is a technique that is based on heat transfer from Kanthal, a part of the Sandvik group. The heating element is in the material NiCr, Nicrothal, an alloy of Nickel-Chromium [40]. The NiCr alloy has the emissivity $\varepsilon = 0.75$

and the heater has a wavelength peak at $\lambda_{peak} = 2.4\mu m$.

This technique is supposed to have a very good absorption ability of water, polymers etc. The temperature of the heating element is lower than for the other types of heaters and have a maximum temperature below 1000 °C.

The heaters are delivered from Opranic where the technique of IR-X is the most common. This is due to the fact that it is emitting less visible light than other techniques, as halogen for example.

All the specifications can be seen in Table 3, [41].

Table 3: Specifications of the different heaters.

	IR-X	**Halogen**	**Carbon**
Material	NiCr	Tungsten	Carbon fibre
Wavelength peak	2.4 μm	1.4 μm	2.0 μm
Emission factor	0.75	0.3	0.77
Maximal temperature heater	1000 °C	2000 °C	1200 - 1300 °C
Power	2.6 kW	2.6 kW	2.6 kW
Length of heater	587 mm	507 mm	570 mm

4.2 Test objects

For the experiments two types of test objects were implemented, plates of fiberglass and a blade section, see Figure 22. In total was four plates used and all of them had a size around 1.5 x 0.5 m and a thickness of 10 mm. For the test plates the gel coat is unknown.

The blade section is from an offshore wind turbine located in Denmark. The section is 2 m long, has a chord length of 1.2 m and weighs 87 kg. The surface of the blade has a gel coat called Mankiewicz.

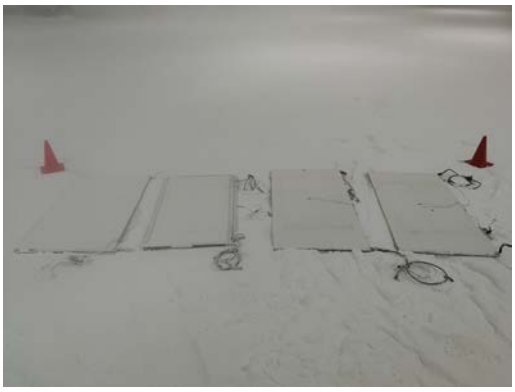

(a) Fiberglass plates.

(b) Blade section.

Figure 22: Test objects.

4.3 Thermal camera

A thermal camera uses thermography to create a heat map and converts far infrared radiation to visible light. In this project a Testo 875i thermal camera, see Figure 23, with an electromagnetic spectrum of 8 - 14 μm was used. It is the surface temperature that is recorded by the thermal camera and the emissivity is adjusted manually depending of the object. For large differences in emissivity between the test object and the surroundings some measurement errors may occur. If measurements is performed outside, without heavy clouding, the sun or a cold atmosphere could be a source of error [42][43].

The data output have the file format *.BMT and contains a thermal image matrix and a regular picture. These files can be converted to *.xslx, *.jpg and *.png files in the Testo software, IR-soft, that also could be used for some image processing. For further analyse of the heat chart the *.xslx file can be imported in MATLAB. The camera can be mounted at a regular tripod and the user needs to manually trigger the camera for each picture [42].

Figure 23: Thermal camera, Testo 875i.

4.4 Thermocouple

To measure temperature, thermocouples can be used. There are different types available of thermocouples available and in this experiment type K has been implemented. The temperature range for this type is –15 to 105 °C. The cable consist of two wires, green is positive and white is negative [44].

4.5 Tension load cell

For the measurements of the ice weight a tension load cell is used. The melting is recorded with the load cell and the test object as a hanging load. For this purpose a load cell of type S-beam model VZ101BH with a range up to 300 kg is implemented, see Figure 24a [45][46].

The load cell is built-up by four strain gauges in a Wheatstone bridge, see Figure 24b, that measure tensile or compression force depending on the application [47]. For this application the tensile force is of interest. Due to the placement of the strain gauges there are no measurement error caused by unwanted heating of the load cell because all of them are affected in the same way and thereby natural compensated [48].

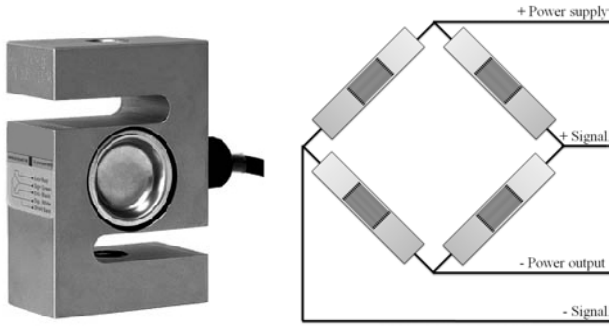

(a) Model VZ101BH. (b) Wheatstone bridge.

Figure 24: Tension load cell.

In Table 4 the colors of the cables from the load cell are presented for the coupling. This specific load cell, VZ101BH, demands an input power supply of 5 V and has a sensitivity of 2 mV/V. It is made of nickel plated steel and can be connected to a shackle or a hank [45][46]. The data sheet for the load cell can be found in Appendix E.

Table 4: Cable colors for the load cell, VZ101BH.

+ Power supply	Red
+ Signal	Green
- Power output	Black
- Signal	White

4.6 Data acquisition

To gather the output data from thermocouples and the tension load cell an analog input module and a computer are needed. In this experiment the National Instrument Data Acquisition model 9219 (NI-DAQ 9219) module is implemented. Different couplings of the signals are required depending on the type of measurements and four separate measurements per module can be done at the same time. In Figure 25 the pinout is shown for NI-DAQ 9219 and Table 5 and 6 gives the signals by mode and describes the signals [49]. For data-logging the software SignalExpress, own by National Instrument, or MATLAB can be used interactive with a NI-DAQ 9219. For the power demand for the sensor an external power supply need to be used.

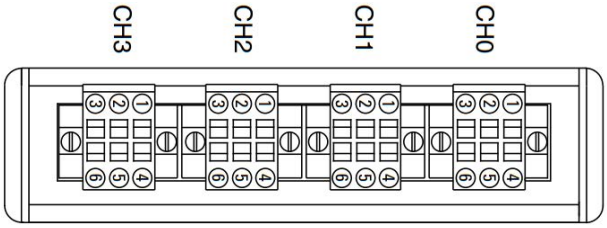

Figure 25: Pinout for NI-DAQ 9219.

Table 5: Signals by mode for NI-DAQ 9219.

Mode	**Pin**					
	1	2	3	4	5	6
Thermocouple	T+	T-	-	HI	LO	-
Voltage	T+	T-	-	HI	LO	-
Current	T+	T-	HI	-	LO	-

Table 6: Signal description for NI-DAQ 9219.

Signal	**Description**
EX+	Positive sensor excitation connection.
EX-	Negative sensor excitation connection.
HI	Positive input signal connection.
LO	Negative input signal connection.
T+	TEDS data connection.
T-	TEDS COM connection.

4.7 Thermopile sensor

A thermopile sensor is a device that converts thermal energy into electrical energy. The instrument is consisting of several thermocouples that is usually connected in series but sometimes in parallel as well [50]. The sensor is measuring the temperature difference between an absorbent surface, that works as a blackbody, and thermocouples [40][50]. A graphic sketch in Figure 26c shows the principle of how a thermopile is built.

The sensor that was used was a Low Power Thermal Sensor type 10 A from Ophir, see Figure 26b. The sensor has a spectral range of 0.19 - 20 μm and a power range of 10 mW - 10 W. The diameter of the absorber is 16 mm [51].

Together with the thermopile sensor a measurement device, NOVA II from Ophir, were used.

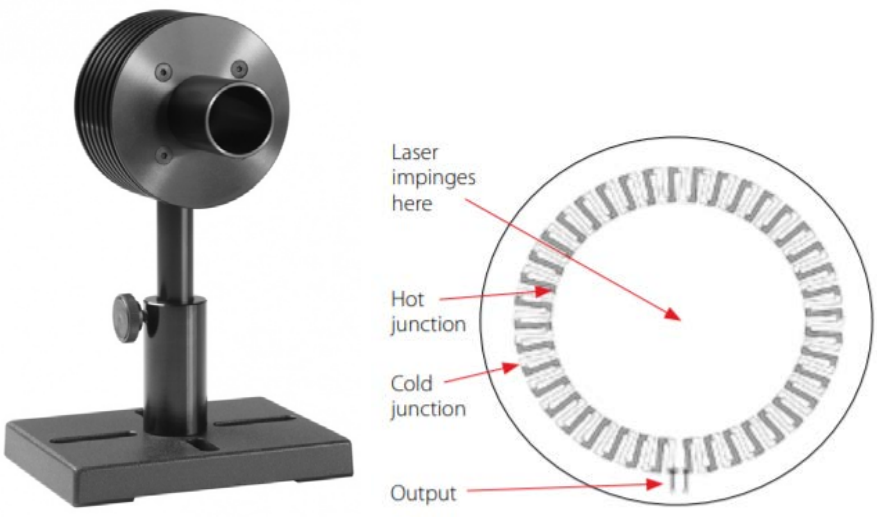

(a) Sensor from Ophir [51]. (b) Illustration of the thermopile sensor.

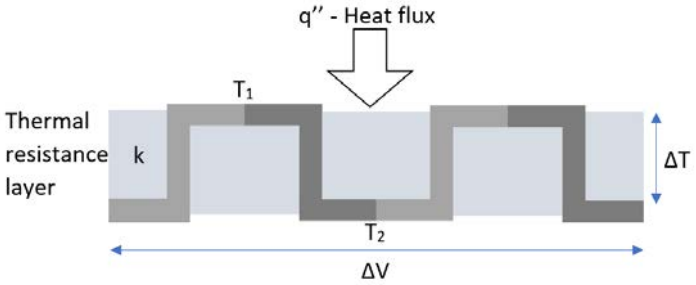

(c) Graphic illustration of how the thermopile is built.

Figure 26: Thermopile sensor.

5 Methodology

The methodology for the experiments is described in this section and a description of the equipment's is found in Section 4. Literature studies have been done as a start of the project and includes articles, technical reports and books in the subject. Before performing any experiment a risk assessment was done and is described in Section 5.1.

The setup and implementations for the different experiments are presented in Section 5.3 and 5.4. A definition of the de-icing time and other parameters are included in Section 5.5.

The experimental timeline started with the small scale glaze ice tests for a first evaluation of the different infrared heaters. From the first results a test matrix and combinations of wavelengths for the following tests could be designed. The test with snow independent of the scale was performed alternately while the intensity tests was performed independently and is described in Section 5.2.

5.1 Risk assessment

Before any experimental work a risk assessment were done to find and minimize potential risks with the experiments. The risk assessment was done as requested by Vattenfall R&D and the full risk assessment can be find in Appendix F.

Some of the potential risks and actions:

- Lack of electrical knowledge/education - Hires an electrician.
- No defined work place, stationary work - Regular breaks.
- Heavy machinery in movement close by - Communication and awareness, safety clothes.
- Risk of slippery ground due to ice - Remove ice if possible, use sand.
- Risk of falling blade - Make sure that the blade is mounted correct.
- High temperature surface, infrared heater - Awareness, suitable gloves.
- Work with electromagnetic radiance, infrared radiation - Avoid looking into the heater, use glasses.

- Electrical equipment close to water - Avoid unnecessary contact with water and keep the equipment above ground. Use a residual-current circuit breaker.
- Transport by car, driving - Rest before driving, see other possibilities, consider going by bus.

5.2 Intensity of radiation

To measure how intense the radiation is for the different heaters, tests with a thermopile sensor were done. The intensity of the heaters is a way to evaluate how efficient the radiation from the specific heater is. The intensity measurements were tested for different distances to get a knowledge of how the intensity decreases with the distance. To perform the tests, a thermopile sensor and a measurement device Ophir Nova II was used. The experimental setup is seen in Figure 27.

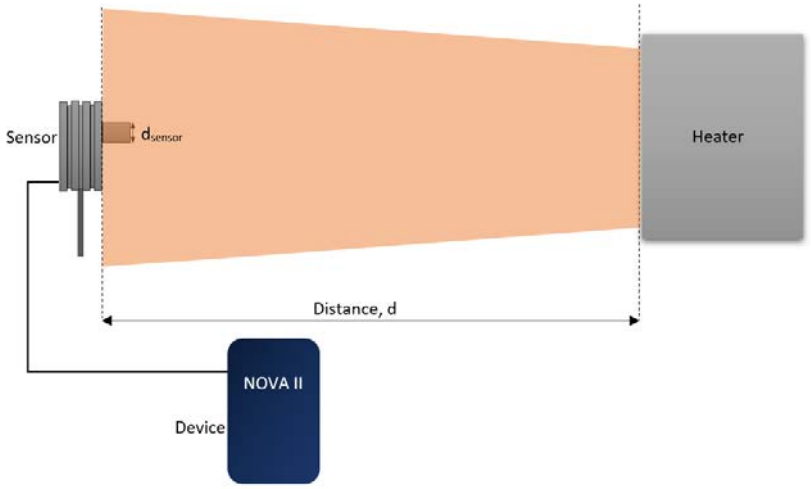

Figure 27: The setup for the experimental test with a thermopile sensor.

5.2.1 Single heater, 2.6 kW

The test was performed by varying the distance, d, in steps of 0.2 m, from 1 m to 0.2 m. Within every distance the intensity of the the radiation was measured. A value of the power in watt was received from the NOVA II device and noted when the value had stabilised for the type of heaters and

the distance. The thermopile was placed in the middle of the heaters and only moved in the direction of the distance, d.

Because the thermopile sensor is measuring the difference in high and low temperature, two different tests were done. One test was with a shield and small pipe to avoid heating up the sensor. The shield was in a thin aluminum material and blocked out all the light that was going outside the blackbody absorber. The other test was without the shield and the pipe but was done quickly so the sensor did not heat up.

5.2.2 Multiple heaters, 7.8 kW

The same type of tests were done with the two different combinations of heaters. This time the measurements were performed at nine points distributed over an area, 2x2 m. The purpose of this tests was to see how the intensity was distributed over the surface and to determine the radiated power that reached the surface. In the same way as for the single heater test, the measurements were performed at different distances from 1 to 5 m to determine the relation between the power and the distance for the two different combinations of heaters. The measured points are distributed over the surface as seen in Figure 28.

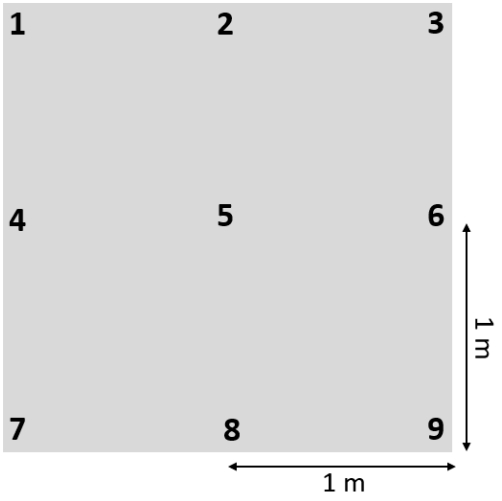

Figure 28: Measured points over a 2x2m surface.

The test matrix for the intensity tests for the two combination of heaters was as seen in Table 7. The numbers 1-9 are the points distributed as in Figure

28.

Table 7: Test matrix for the different points for different distances, X marks a measured point.

Distance [m]	1	2	3	4	5	6	7	8	9
1	X	X	X	X	X	X	X	X	X
1.5	-	-	-	-	X	-	-	-	-
2	X	-	X	-	X	-	X	-	X
2.5	X	-	X	-	X	-	X	-	X
3	X	X	X	X	X	X	X	X	X
4	X	X	X	X	X	X	X	X	X
5	-	-	-	-	X	-	-	-	-

5.3 Small scale tests

The purpose of the small scale tests was to evaluate the infrared heaters with different wavelengths in different surrounding temperatures. This was performed for two different types of ice, glaze ice and snow, and the ice build-up and experimental setup is explained in the two coming sections for each type.

5.3.1 Glaze ice build-up

To be able to create a thick layer of glaze ice on a surface a method for ice build-up was made. The material that was used was plastic boxes (40x50 cm), seals and smooth plastic tape. The box was placed up side down and a hole was created in the bottom to be able to pour water in the box, see Figure 29a. Seals were placed on the edge of the box. Plastic tape with a smooth surface was taped on to the sides to avoid the ice to attach to the surface of the box.

A thermocouple was placed and taped at the surface of the plate. To start the ice build-up some water was sprayed at the surface before the box was placed on the plate. Water was poured inside the box to approximately 1 cm depth. Putting some pressure on the box sealed the surfaces against each other.

When the water was totally frozen the plastic box was removed. Because of that water expands when it freezes to ice, it had formed some cracks in

the ice. If the ice was fully cracked and pieces were released from the blade, the pieces were attached back to the blade while spraying water between the surfaces. An example of a final sample of ice is shown in Figure 29b.

(a) Ice build-up in the making. (b) Finished sample of ice.

Figure 29: Ice build-up procedure for small scale tests with glaze ice.

5.3.2 Glaze ice, experimental setup

The tests were performed in a climate chamber at Luleå University of Technology. The chamber was about 12 m^2 and height of 2 m. The settings for the freezer was the temperature -5 °C.

The instruments and material used in the experiments were a thermal camera to capture the melting sequences of the ice, thermocouples to measure the temperature of the blade and chamber. Except the instruments, plates made of fiberglass and epoxy were used. The plates have a surface that is similar to the surface of a wind turbine blade. A schematic view of the setup is shown in Figure 30.

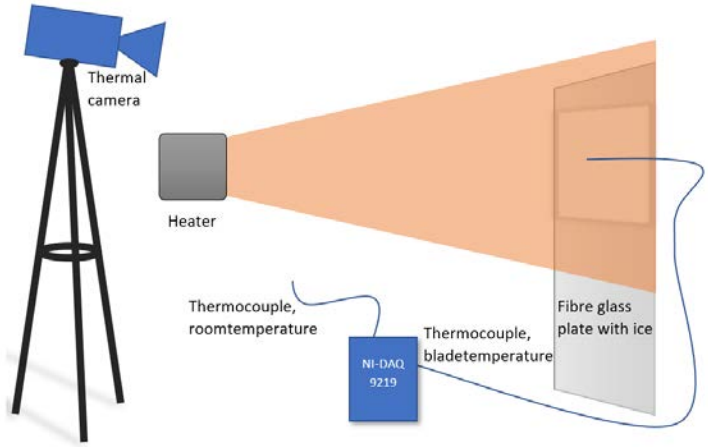

Figure 30: Experimental setup for the small scale tests.

The heater was placed on a metal wagon with clamps holding the heater at place. To determine the mass that was melted, plastic boxes were used to collect the melt water. The plastic boxes also worked as a stand for the plates to be centred in front of the heaters. The distance between the heaters and the plate was measured thoroughly before the test started. In Figure 31a and 31b the setup in the freezer is showed.

The test was started when the heater was plugged in. A first picture with the thermal camera was taken right before test started and right after the test was started. After the first pictures, pictures were taken every 30 second with the thermal camera.The temperature from the thermocouples was logged with a sampling frequency of 1-2 Hz. Except for the pictures, notes were taken for characteristic occurrences as cracks or pieces that were falling from the blade. When the plate was fully de-iced, the heater was turned off to cool down. The melt water was then weighed.

(a) The setup with camera, heater and blade.

(b) The blade with plastic boxes to collect melt water.

Figure 31: Experimental setup in the freezer.

5.3.3 Snow build-up

For the creation of an artificial rime ice a snow machine was used. The fiberglass plates were placed laying on the ground with a gentle slope in front of the snow machine, see Figure 32. The settings for the machine was set do a water flow of 150 liter/hour with a low speed of the fans that gave a wet snow. When the snow layer was about 1 cm the plates was left resting on the ground for a few hours in the cold.

Figure 32: Snow build-up for small scale tests.

5.3.4 Snow, experimental setup

The experimental setup for the small scale test with snow in two different temperatures are shown in Figure 33. For the experiments one heater at the time was tested and the heaters were placed vertical in a frame. Temperature measurements were made with a thermal camera and the surrounding temperature was set to -15 °C respectively -30 °C. Pictures were taken with the thermal camera every 10 second together with a picture taken the minute before the experiment. The distance between the fiberglass plate and the heater was set to 0.5 m. After every finished test the plates and the deiced surface was documented. This experiments were performed in a climate chamber in Arctic Falls facilities in Piteå.

Figure 33: Experimental setup for the small scale test with snow.

5.4 Full scale tests

The full scale tests were performed on a blade section from a real wind turbine blade. The location for the test was a climate hall (10 000 m^2) in Arctic Falls facility that is located in Piteå. The purpose was to test different the different combinations of heaters and to determine how the distance affected the de-icing time. Methodology for the full scale experiments is described below.

5.4.1 Snow build-up

To create the snow at the blade section the blade was lowered to the ground with an angle, as seen in Figure 34, in front of the snow machine. Two different snow types was tested by changing the water flow which was used for the test samples for the full scale tests. The first snow was a dryer snow with the machine sat to 350 liter/hour and the second snow was a wetter snow where the machine was sat to 150 liter/hour and almost no fan. The snow machine operated for 30-60 minutes and then the blade got to rest for a few hours so the snow would be totally frozen.

Figure 34: Snow build-up for the full scale tests.

5.4.2 Experimental setup

For the full scale tests three heaters were used at the same time but in two different combinations to de-ice the blade section. The frame with the heaters was placed on large wooden cable reels in front of the hanging blade as seen in Figure 35a. For the suspension of the blade a lift was used together with a load cell and straps made for lifting. A closeup of the suspension is seen in Figure 35b. The load cell was connected to a NI-DAQ for data collection. For measurements of the heat distribution a thermal camera was implemented. To make sure that no ice would accumulate inside the blade and give an inaccurate measurement of the weight, the top of the blade was sealed with plastic.

(a) Hanging blade, heaters and thermal camera.

(b) Close up of the load cell and suspension device.

Figure 35: Experimental setup for the full scale tests.

5.5 Definitions

Explanations for the different definitions that is used to present the results for the experiments. Depending of the type of experiment the definition of a specific parameter could vary and this is explained in this section. The calculations behind the definitions can be seen in Section 3.3 for a more mathematical explanation.

5.5.1 Total test time

Small scale, glaze ice

The test continued until the fiber glass plate was totally de-iced as observed by the person performing the test.

Small scale, snow

The test continued until the surface of the fiber glass plate reached a maximum temperature of 40 °C, due to recommendations from the manufacture, or a total test time of maximal 20 min, due to the cold working environment.

Full scale

The test continued until the surface of the blade section reached a maximum temperature of 40 °C, due to recommendations from the manufacture.

5.5.2 Time of de-icing

Rapid change in temperature

Time of de-icing decided by when the temperature starts to raise quickly after being stable around 0 °C.

Abrupt decreasing of melting

Time of de-icing decided of when the weight of the blade start to stabilise and the melting stops.

Total test time

Time of de-icing set to the total time due to a high amount of ice left on the surface and thereby only a partly de-iced surface.

By-eye

Time of de-icing observed by the person performing the test. Could be done afterward from the images collected with the thermal camera. Also used as a control for the other definitions for time of de-icing.

5.5.3 Time of start sequence

Time of the sequence before the surface reached an average temperature of 0 °C.

5.5.4 Melting rate

The melting rate is describing the melted snow weight per minute.

5.5.5 Temperature gradient

The temperature gradient is the mean value of the slope in the end of the test when the average maximum temperature raised quickly.

5.5.6 Efficiency

The efficiency is based on the intensity measurements for the respective combination of heaters and the conditions of the snow surface as weight and heat capacity. The quota between the energy that is required to melt the specific mass of the ice and the energy that is radiated on the blade surface.

5.6 Modeling

A simple model was created to visualise how the de-icing system could be implemented and used if it is applied on a real case and a real wind turbine. The model is based on the results from the measurements that has been performed during the project. The results gives an estimation of how the de-icing time is affected by the different combination of heaters at different distances. A flow chart for how the model is designed is presented in Figure 36

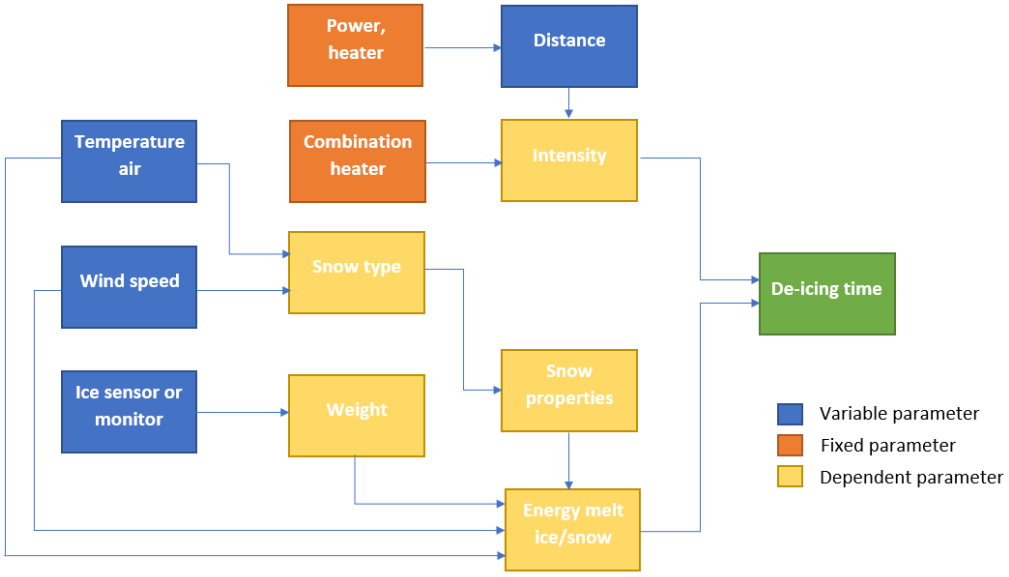

Figure 36: A block diagram of how the model is created.

6 Results

In this section results from theory and method are presented. First a summary of the measured and calculated values for intensity of radiation divided in single heater and multiple heaters is included (Section 6.1). Then the results of the small scale tests for glaze ice (Section 6.2) and snow (Section 6.3) is presented followed by the full scale results (Section 6.4).

6.1 Intensity of radiation

The measured values and the results from the thermopile sensor is presented in this section. The measurements was made for one heater at a time, 2.6 kW and with three heaters, 7.8 kW, in two different combinations.

6.1.1 Single heater, 2.6 kW

Measured values from the thermopile sensor can be seen in Table 8.

Table 8: Values from the intensity measurements for the heaters.

	IR-X [W]		**Carbon [W]**		**Halogen [W]**	
Distance	Shield	No shield	Shield	No shield	Shield	No shield
1.0 m	0.17	0.13	0.15	0.13	0.17	0.14
0.8 m	0.24	0.21	0.2	0.18	0.27	0.23
0.6 m	0.37	0.34	0.3	0.28	0.41	0.39
0.4 m	0.58	0.63	0.5	0.52	0.74	0.82
0.2 m	1.27	1.5	1.11	1.22	no value	no value

Dividing the values in Table 8 with the area of the blackbody absorber of the sensor gives the intensity of radiation. The intensity can be seen in Figure 37.

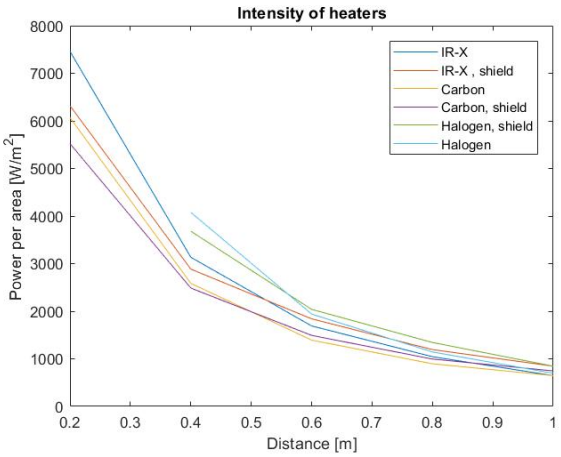

Figure 37: Measured intensity for all the heaters, with and without shield.

Though the heaters have different lengths it means that the intensity is differently distributed. The measurements are only at one point in front of the heater.

6.1.2 Multiple heaters, 7.8 kW

The tests were done with three heaters of type IR-X respectively two IR-X and one Halogen. The measurements was performed as described in methodology, and the values marked as X is points that were not measured.

In Table 9 the power for each measuring point for different distances is shown for the combination of three heaters of type IR-X, $\lambda = 2.4\mu m$, from now on referred to as combination 1.

Table 9: Measured values for the intensity for the heater combination with three IR-X.

Distance [m]	1	2	3	4	5	6	7	8	9
1	0	0.01	0	0.01	0.33	0.01	0	0.02	0
1.5	X	X	X	X	0.17	X	X	X	X
2	0.02	X	0.02	X	0.09	X	0.02	X	0.02
2.5	0.01	X	0.02	X	0.06	X	0.02	X	0.03
3	0.02	0.03	0.03	0.03	0.04	0.02	0.02	0.03	0.03
4.15	0.01	0.02	0.02	0.02	0.02	0.02	0.02	0.02	0.02
5	X	X	X	X	0.02	X	X	X	X

From the table, it is clearly shown that the radiation is not evenly distributed over the surface. To determine how the radiation and power is distributed a bilinear interpolation for some of the distances, where all the points was measured, was made. From this values an image was plotted in Matlab to easier see the distribution over the surface, see Figure 38.

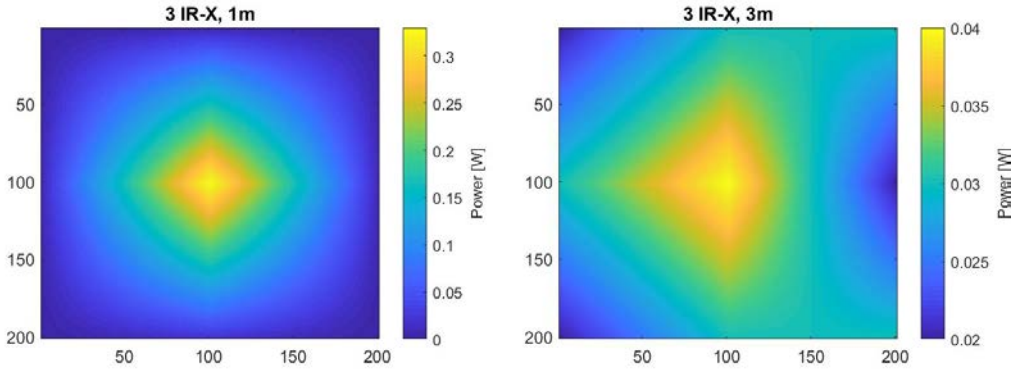

(a) Radiation distribution at 1 m. (b) Radiation distribution at 3 m.

Figure 38: Intensity distribution for heater combination with 3 IR-X.

From Figure 38a the scale on the colorbar displays that the intensity is significant higher in the middle of the surface and decreases out towards the edges. Figure 38b compared to Figure 38a has a more evenly distributed radiation but a lower total radiation power, seen from the scale on the colorbar. But still it is even here noticeable that the radiation is more concentrated to the middle of the surface.

The values from the calculated data was summarised and plotted against the distance to see how the radiation power on the surface decreases with the distance, see Figure 39. The radiated power was calculated with an exponential fit.

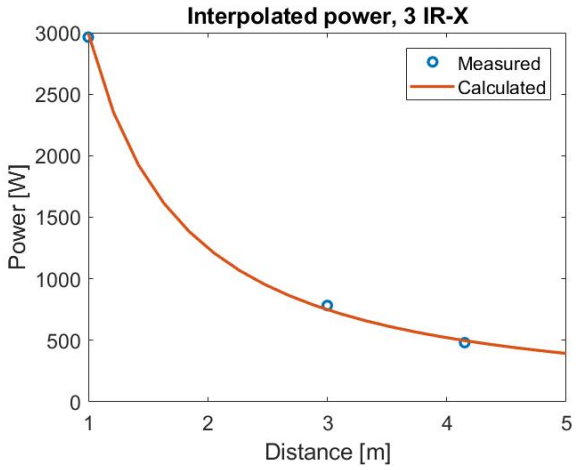

Figure 39: Power for different distances for the heater combination with 3 IR-X.

As seen in Figure 39 the power decreases fast in the beginning, for the shorter distance to then have a more stabilise appearance for the longer distances.

The measured values for the combined heaters with one Halogen and two IR-X, $\lambda = 1.4\mu m$ and $\lambda = 2.4\mu m$, from now on referred to as combination 2, is shown in Table 10.

Table 10: Measured intensity values for the combined heaters.

Distance [m]	1	2	3	4	5	6	7	8	9
1	0.0	0.02	0.0	0.02	0.34	0.02	0.01	0.02	0.01
1,5	X	0.04	X	0.06	0.16	0.06	X	0.03	X
2	0.04	X	0.03	X	0.1	X	0.02	X	0.01
2.5	0.02	X	0.03	X	0.06	X	0.02	X	0.02
3	0.02	0.03	0.02	0.03	0.05	0.02	0.02	0.03	0.02
4	0.02	0.02	0.02	0.02	0.02	0.02	0.02	0.02	0.02
5	X	X	X	X	0.02	X	X	X	X

In the same way as for combination 1, images for the distribution was plotted, see Figure 40.

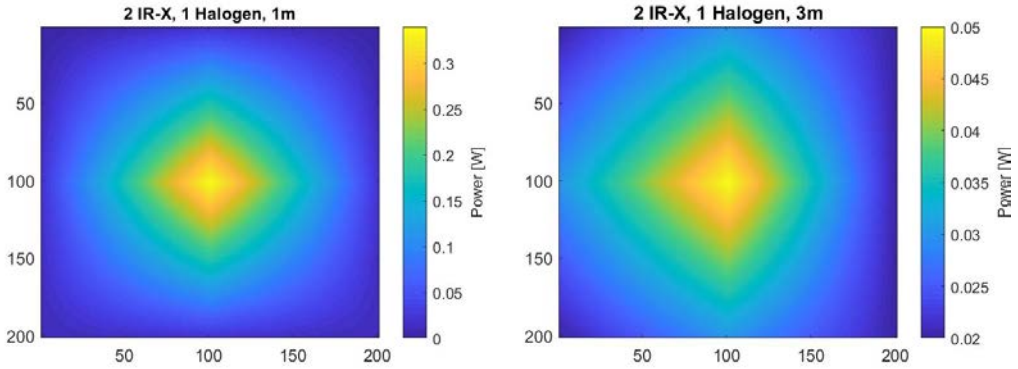

(a) Radiation distribution at 1 m. (b) Radiation distribution at 3 m.

Figure 40: Intensity distribution for heater combination with 2 IR-X and 1 Halogen.

Similar to Figure 40a the intensity in Figure 40a is higher in the middle of the surface and decreases fast out towards the edges, yet not as much as for combination 1.

For the longer distance the intensity in Figure 40b is more distributed over the surface compared to 40a but still have a more concentrated spot in the middle.

The total radiated power on the surface for different distances is seen in Figure 41.

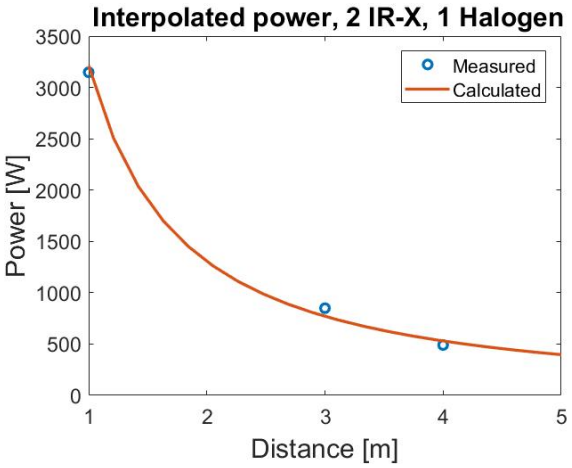

Figure 41: Power for different distances for the combined heater with 2 IR-X and and 1 Halogen.

6.2 Small scale, glaze ice

The results for the small scale experiments with glaze ice are shown in Table 11. The table shows a comparison between the different heaters with different wavelength peaks. An explanation of the calculations and definitions can be seen in Section 3.3 and 5.5. Heat charts together with images are presented in this section for Test B (Section 6.2.1) and Test E (Section 6.2.2). Figures for Test A, C and D are presented in Appendix G.

Table 11: Comparison of infrared heaters with a power of 2.6 kW for glaze ice.

	Test A	**Test B**	**Test C**	**Test D**	**Test E**
Heater	IR-X	IR-X	Halogen	Carbon	Halogen
Wavelength peak	2.4 μm	2.4 μm	1.4 μm	2 μm	1.4 μm
Ice thickness	9.9 mm	7.8 mm	10.5 mm	12.4 mm	11.6 mm
Ice weight	1 817 g	1 560 g	2 104 g	2 482 g	2 135 g
Type of ice	Glaze ice	Glaze ice	Glaze ice	Glaze ice	Glaze ice
Type of de-icing	Melting ice	Melting ice	Warming blade	Melting ice	Warming blade
Distance	1 m	0.5 m	0.5 m	0.5 m	0.5 m
Test time	105 min	38 min	29 min	60 min	10 min
De-icing time	75 min	30 min	25 min	45 min	8.5 min
Time, start sequence	6 min	3.5 min	3 min	3.5 min	3 min
Energy, heat $[Q_{heat}]$	17.2 kJ	20.04 kJ	26.7 kJ	42 kJ	43.7 kJ
Energy, latent $[Q_{latent}]$	607 kJ	521 kJ	703 kJ	829 kJ	719 kJ
Energy, melt $[Q_{melt}]$	624 kJ	541 kJ	729 kJ	871 kJ	763 kJ
Power, melt $[P_{melt}]$	139 W	301 W	420 W	313 W	1 292 W

Blade and room temperatures measured with the thermocouples can be seen in Figure 42 for Test B, C and D.

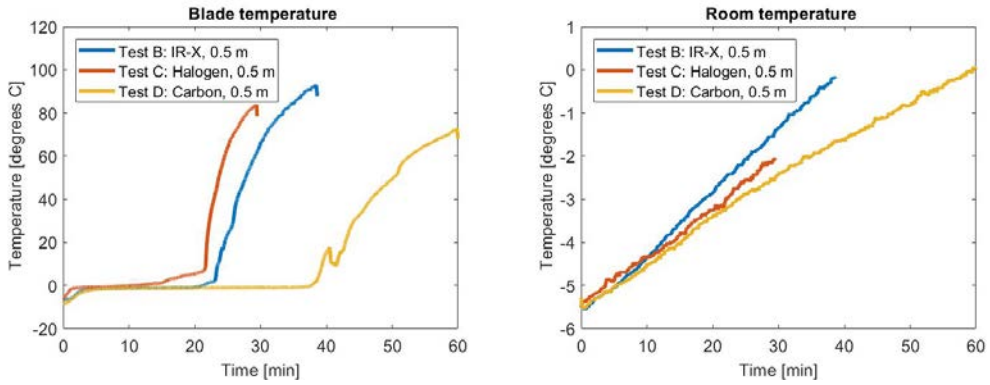

(a) Blade temperature. (b) Room temperature.

Figure 42: Temperatures measured with thermocouples for Test B,C and D.

Minimal and maximal temperatures at the surfaces measured with the thermal camera are shown in Figure 43. The start sequence is visualised in Figure 43a where the temperature rises to 0 °C in the beginning and then stays stable until the blade is totally de-iced for the small scale experiments with glaze ice.

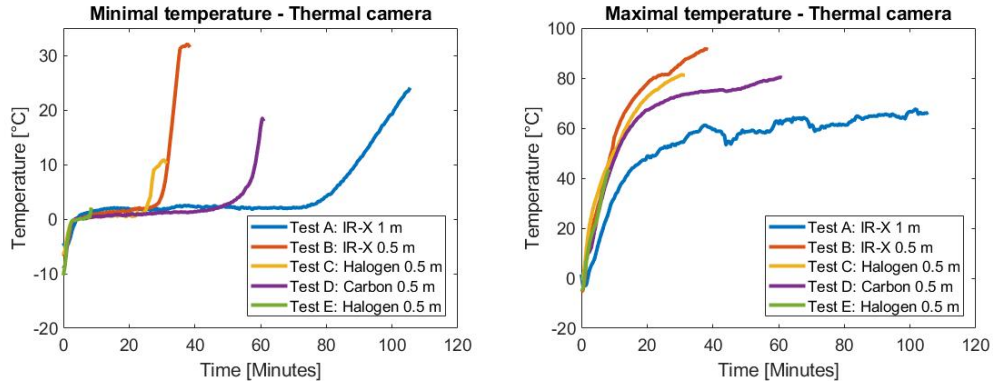

(a) Minimal temperature. (b) Maximal temperature.

Figure 43: Temperature at the surface of the ice and fiberglass plate measured with the thermal camera.

6.2.1 Test B: IR-X at 0.5 m, glaze ice

This test was performed with the IR-X heater at a distance of 0.5 m. In Figure 44 heat charts are shown for different time steps from the experiment. The ice sample is placed horizontal and in Figure 44a cracks in the ice are

seen at the start. The melt water started poring quickly after the heater was turned on. Observed during the experiment was that the ice braked some more in the edges when 1-2 min had passed, but it did not drop down from the plate. After 20 min, small pieces of ice dropped down from the plate. The end of stability sequence is 30 min and Figure 70g shows that the ice is melted.

(a) Image, start.

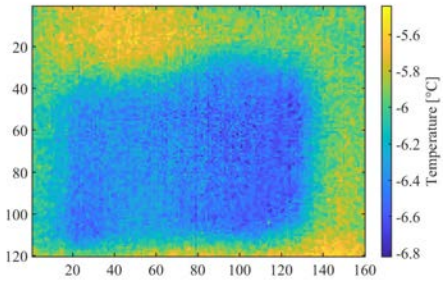

(b) Heat chart, start.

(c) Image, 5 min.

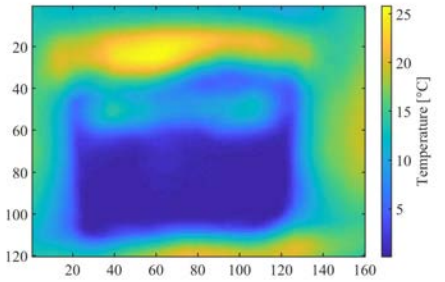

(d) Heat chart, 5 min.

(e) Image, 20 min.

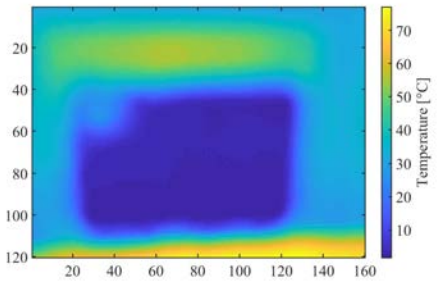

(f) Heat chart, 20 min.

(g) Image, 30 min.

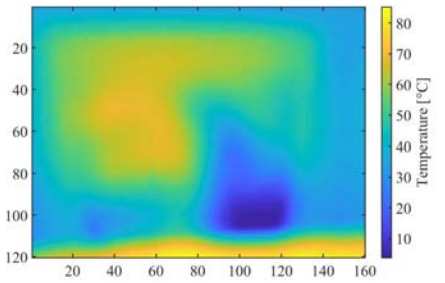

(h) Heat chart, 30 min.

Figure 44: Images and heat charts in time sequences for Test B, IR-X 0.5 m, glaze ice.

6.2.2 Test E: Halogen at 0.5 m, glaze ice

This test was performed with the Halogen heater at a distance of 0.5 m. In Figure 45 heat charts are shown for different time steps from the experiment. The ice sample was placed horizontal and in Figure 45a some cracks in the ice are seen at the start. A water layer between the ice and the plate starts forming directly after the heater was turned on. Figure 45e shows that ice has fallen down to the ground.

(a) Image, start.

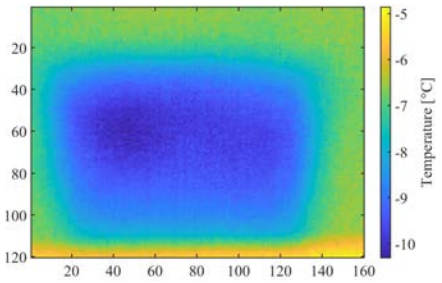

(b) Heat chart, start.

(c) Image, 5 min.

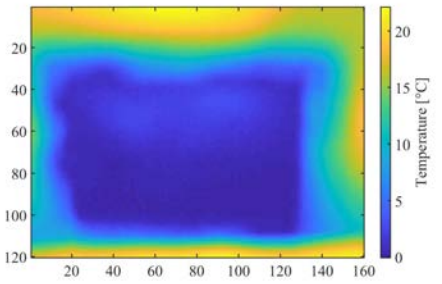

(d) Heat chart, 5 min.

(e) Image, 8.5 min.

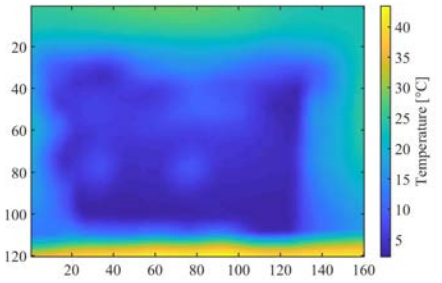

(f) Heat chart, 8.5 min.

Figure 45: Images and heat charts in time sequences for Test E, Halogen 0.5 m, glaze ice.

6.3 Small scale, snow

Measured values for the small scale experiment with snow, that is similar to rime ice, with two different temperatures are shown in Table 12. The experiments were stopped when the surface reached a maximal temperature of 40 °C or a total test time of 20 min. All equations used for the calculations can be seen i Section 3.3 and definitions are explained in Section 5.5.

Table 12: Comparison of infrared heaters with a power of 2.6 kW for snow.

	Test F	**Test G**	**Test H**	**Test I**
Heater	Halogen	IR-X	IR-X	Halogen
Wavelength peak	1.4 μm	2.4 μm	2.4 μm	1.4 μm
Surrounding temperature	-30 °C	-30 °C	-15 °C	-15 °C
Type of ice	Snow	Snow	Snow	Snow
Distance	0.5 m	0.5 m	0.5 m	0.5 m
De-icing time	20.5 min	12.8 min	20.3 min	15.3 min
Time, start sequence	40 s	78 s	72 s	20 s

The graph in Figure 46 shows the average temperature variation for the maximal and minimal temperature from the thermal camera.

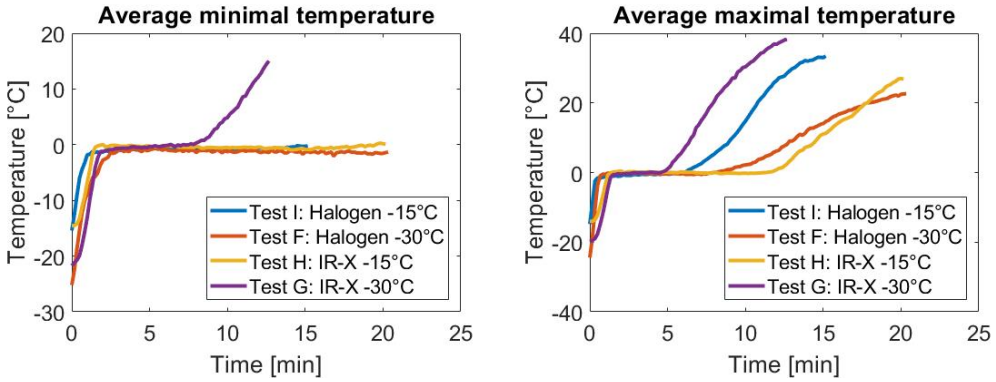

(a) Minimal temperature. (b) Maximal temperature.

Figure 46: Average temperature measured with the thermal camera for Test f,G,H and I.

6.3.1 Test F: Halogen at 0.5 m, snow -30 °C

Images and heat charts for the surface before and after the de-icing experiment for Test F are shown in Figure 47.

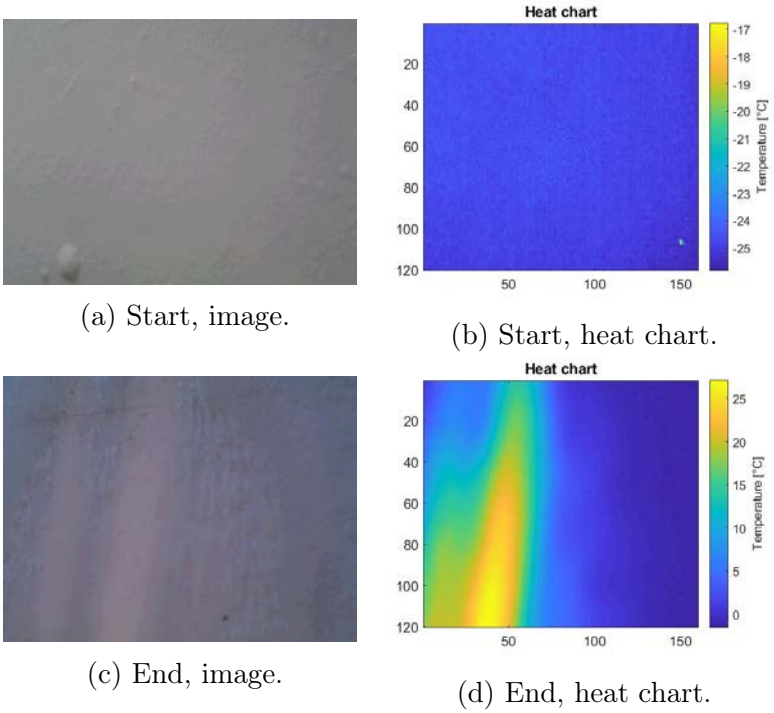

(a) Start, image.

(b) Start, heat chart.

(c) End, image.

(d) End, heat chart.

Figure 47: Images and heat charts in time sequences for Test F, Halogen 0.5 m, snow -30 °C.

6.3.2 Test G: IR-X at 0.5 m, snow -30 °C

Images and heat charts for the surface before and after the de-icing experiment for Test G are shown in Figure 48.

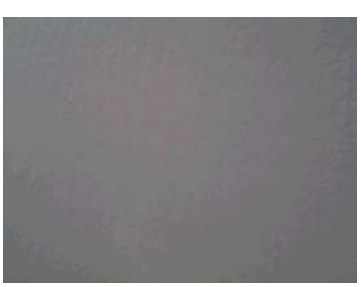

(a) Start, image.

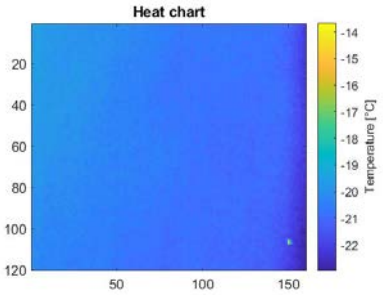

(b) Start, heat chart.

(c) End, image.

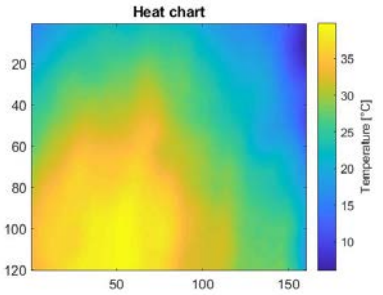

(d) End, heat chart.

Figure 48: Images and heat charts in time sequences for Test G, IR-X 0.5 m, snow -30 °C.

6.3.3 Test H: IR-X at 0.5 m, snow -15 °C

Images and heat charts for the surface before and after the de-icing experiment for Test H are shown in Figure 49.

(a) Start, image.

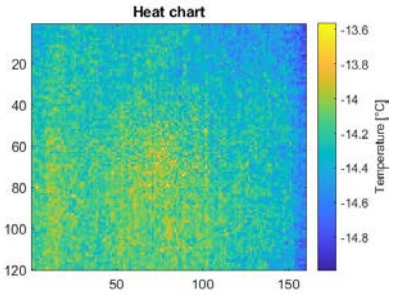

(b) Start, heat chart.

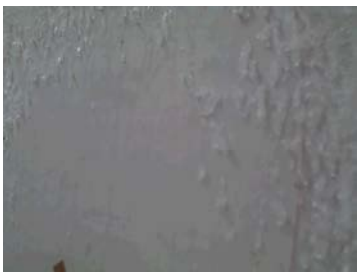

(c) End, image.

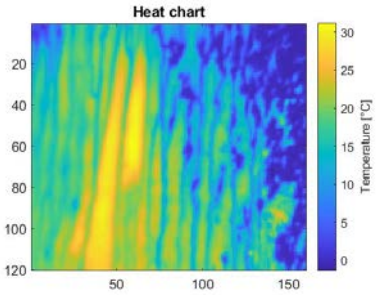

(d) End, heat chart.

Figure 49: Images and heat charts in time sequences for Test H, IR-X 0.5 m, snow -15 °C.

6.3.4 Test I: Halogen at 0.5 m, snow -15 °C

Images and heat charts for the surface before and after the de-icing experiment for Test I are shown in Figure 50.

(a) Start, image.

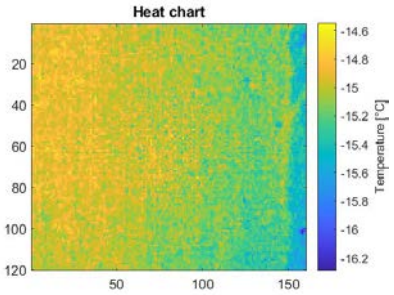

(b) Start, heat chart.

(c) End, image.

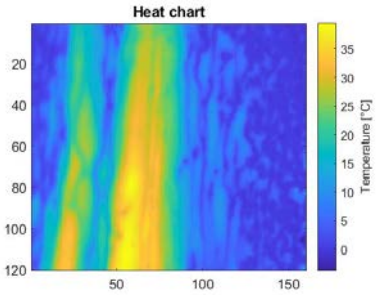

(d) End, heat chart.

Figure 50: Images and heat charts in time sequences for Test I, Halogen 0.5 m, snow -15 °C.

6.4 Full scale tests

The tests performed with the blade section were tested with different variable parameters as distance, combination of heaters and snow type. Some of the most comparable and interesting tests are individually presented in this section. The remaining tests are presented in Appendix H.

All the tests that were performed are summarised in Table 13 and are numbered and referred to as Test 1-9 from top to bottom.

Table 13: All the full scale tests summarised in one table.

Heater combination	Distance [m]	Weight [kg]	Snow type	Time [min]	Melting rate [kg/min]	Efficiency	Temperature gradient
1	1	2.77	Dry snow	14	0.20	37 %	0.92
1	1	4.70	Dry snow	27.3	0.17	32 %	0.57
1	1.5	5.18	Dry snow	40.8	0.13	34 %	0.25
2	1	1.82	Dry snow	13.8	0.16	23 %	0.64
2	1.5	10.15	Dry snow	50.7	0.20	58 %	0.16
2	1.5	7.53	Wet snow	35.6	0.21	62 %	0.24
1	*1.5*	*1.58*	*Wet snow*	*23.7*	*0.07*	*18 %*	*0.34*
1	*1.5*	*3.05*	*Wet snow*	*43.6*	*0.07*	*19 %*	*0.20*

6.4.1 Test 2: 3 IR-X at 1 m, dry snow

The second test was performed at 1 m distance and with 3 heaters of type IR-X, combination 1 in Table 13. The snow surface that was accumulated on the blade can be seen in Figure 51a, Figure 52a and Figure 52b. The full de-iced blade surface is shown in Figure 51b.

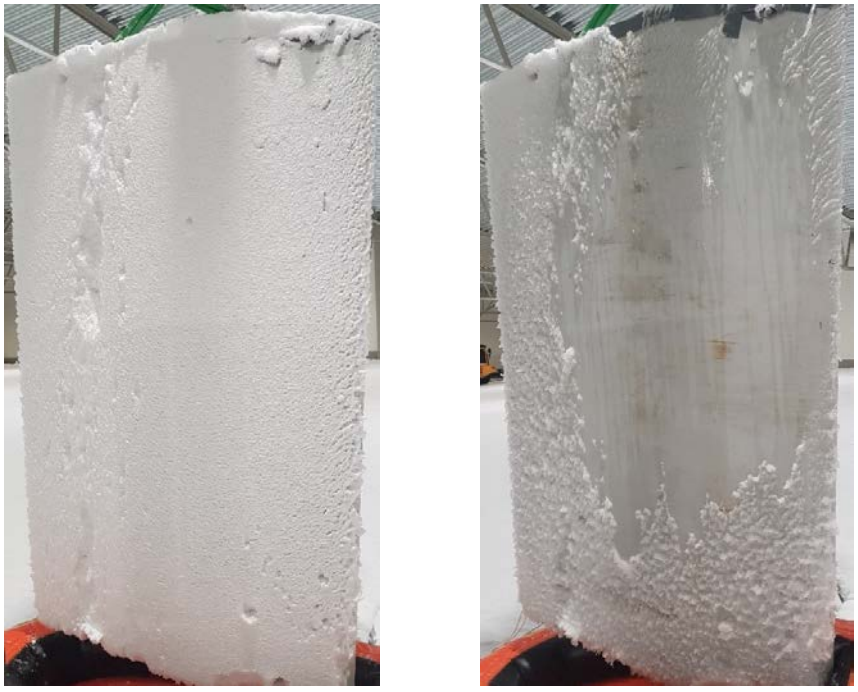

(a) Surface of blade before de-icing. (b) Surface after de-iced blade.

Figure 51: Images of full blade for Test 2.

(a) Trailing edge. (b) Leading edge.

Figure 52: Images of snow on the edges for Test 2.

From the load cell, data was collected to see the snow weight and how the weight was decreasing during the de-icing period. From the thermal camera a maximal average temperature on the surface was calculated, see Figure 53.

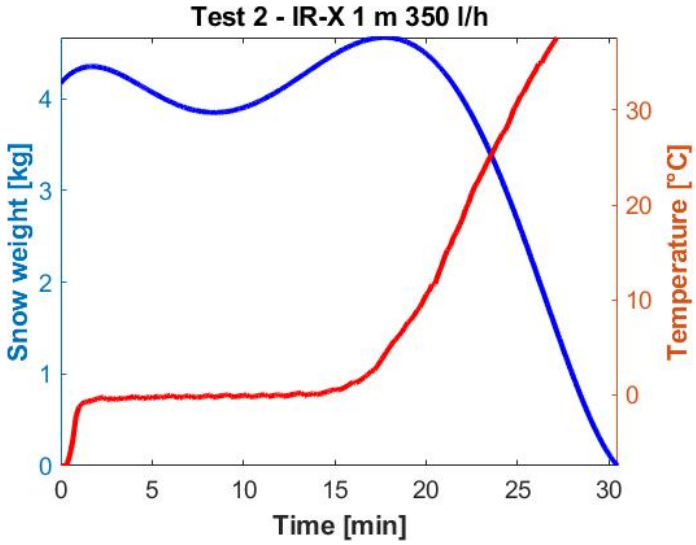

Figure 53: Weight of snow (blue) and maximal average temperature at the surface (red) for Test 2.

6.4.2 Test 3: 3 IR-X at 1.5 m, dry snow

The third test was tested in the same conditions as Test 2 but at a distance 1.5 m. Figures for the snow surface on the blade before de-icing is shown in Figure 54a, Figure 55a and 55b. The de-iced surface is shown in Figure 54b.

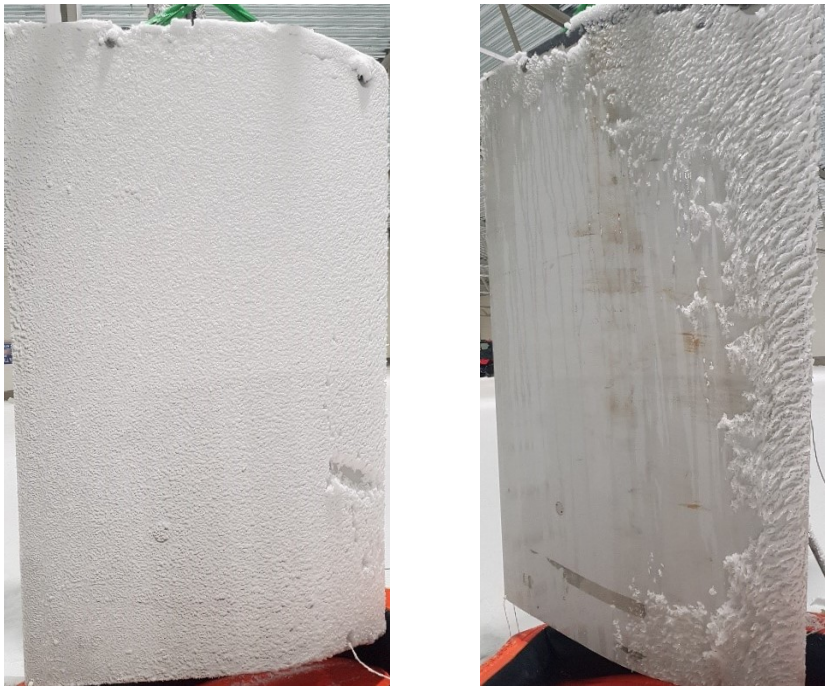

(a) Surface of blade before de-icing. (b) Surface after de-iced blade.

Figure 54: Images of full blade for Test 3.

The snow surface on trailing edge and leading edge.

(a) Trailing edge. (b) Leading edge.

Figure 55: Images of snow on the edges for Test 3.

The graphs for the melting sequence with decreasing weight, load cell, and increasing temperature, thermal camera, is shown in Figure 56.

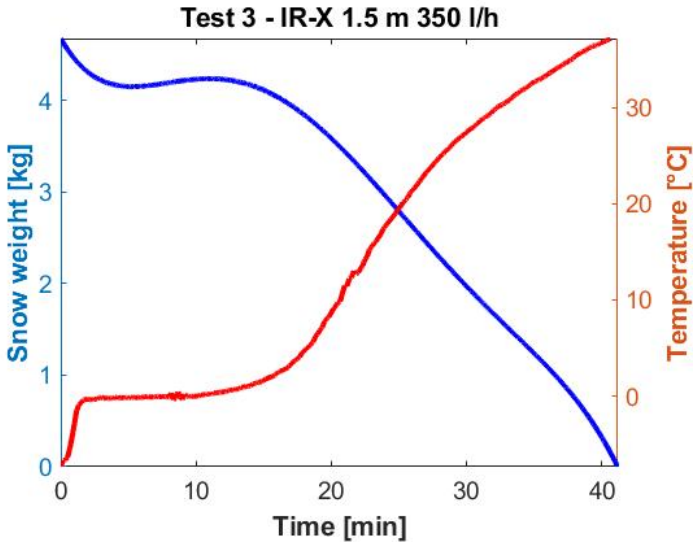

Figure 56: Weight of snow (blue) and maximal average temperature at the surface (red) for Test 3.

6.4.3 Test 4: 2 IR-X & 1 Halogen at 1 m, dry snow

The fourth test performed in the same conditions as for Test 2 but with the combined heaters, combination 2 in Table 13. The snow surface on the full blade are shown in Figure 57a, 58a and 58b. The surface after de-icing is shown in Figure 57b.

(a) Surface of blade before de-icing. (b) Surface after de-iced blade.

Figure 57: Images of full blade for Test 4.

The snow surface on trailing and leading edge.

(a) Trailing edge. (b) Leading edge.

Figure 58: Images of snow on the edges for Test 4.

Data from the load cell for the decreasing weight and the temperature from the thermal camera is shown in Figure 59.

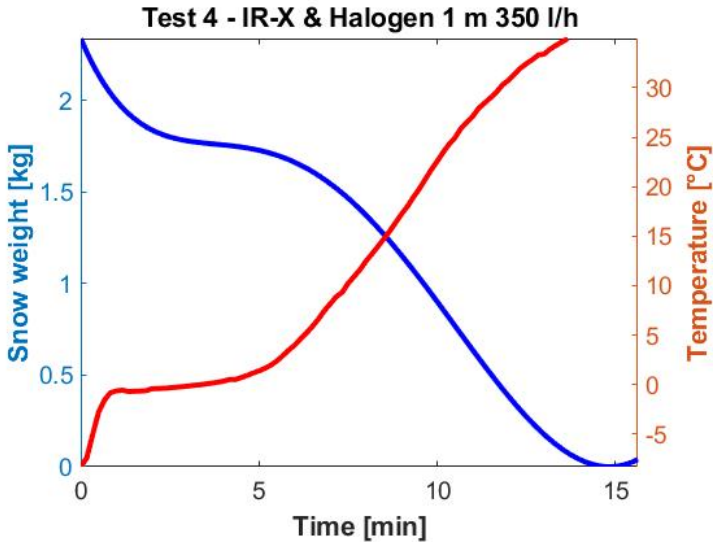

Figure 59: Weight of snow (blue) and maximal average temperature at the surface (red) for Test 4.

6.4.4 Test 5: 2 IR-X & 1 Halogen at 1.5 m, dry snow

The fifth test was with the combined heaters, combination 2, at the distance 1.5 m. The snow surface for the blade is shown in Figure 60a, 61a and 61b. The de-iced surface is shown in Figure 60b.

(a) Surface of blade before de-icing. (b) Surface after de-iced blade.

Figure 60: Images of full blade for Test 4.

Snow surface on trailing and leading edge is shown in Figure 61a and 61b.

(a) Trailing edge. (b) Leading edge.

Figure 61: Images of snow on the edges for Test 5.

The load cell data for the decreasing snow weight and the temperature from the thermal camera is shown in Figure 62.

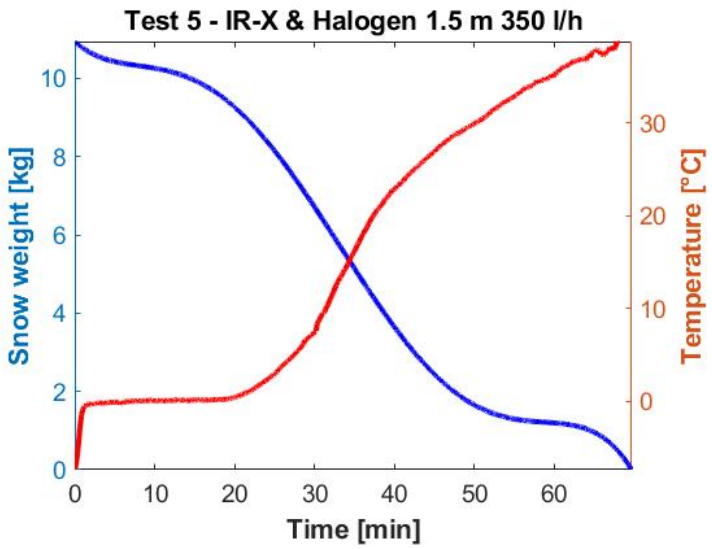

Figure 62: Weight of snow (blue) and maximal average temperature at the surface (red) for Test 5.

6.4.5 Test 6: 2 IR-X & 1 Halogen at 1.5 m, wet snow

The sixth test is tested with a different snow type specified in Section 5.4.1. The snow surface on the blade is shown in Figure 63a,64a and 64b. The full de-iced surface of the blade is shown in Figure 63b

(a) Surface of blade before de-icing. (b) Surface after de-iced blade.

Figure 63: Images of full blade for Test 6.

(a) Trailing edge. (b) Leading edge.

Figure 64: Images of snow on the edges for Test 6.

From the load cell, data was collected to see the snow weight and how the weight was decreasing during the de-icing period.

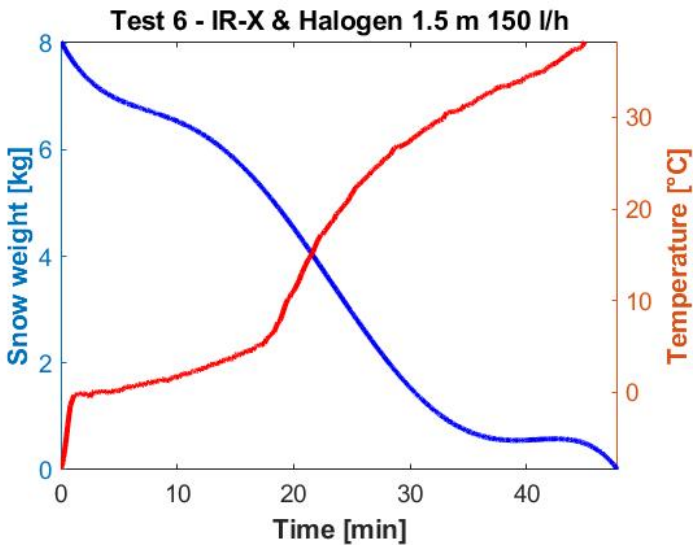

Figure 65: Weight of snow (blue) and maximal average temperature at the surface (red) for Test 6.

6.5 Modeling

To determine how the de-icing time is affected by the variable parameters and how it correlates to the results, a simple model has been designed.

For the two different combination of heaters this will give a relation between the de-icing time per weight of snow and distance as in Figure 66. The Figure is designed and based on a 2 m section of a real wind turbine blade.

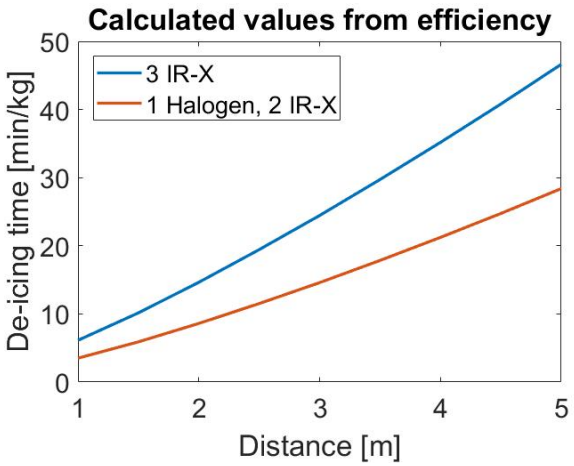

Figure 66: De-icing time in min/kg for different distances (1-5 m) for the two combination of heaters.

If the de-icing method is applied for a wind turbine with 40 m long blades and the power used for the full scale experiments is scaled, the total power needed for the de-icing system is 156 kW ($20 \cdot 7.8$ kW). Based on the experience from the results from the ice build up, it is possible that 4 kg (mean value) of snow is accumulated on blade section that is 2 m long. The weight gives an estimation of how much snow that can accumulate on a full blade, 80 kg of snow per blade.

This gives from values in Figure 66 de-icing time for the first combination of heaters (3 IR-X) that is 63 min/blade ($4 \cdot 15.8$ min/kg). For the same distance and weight the de-icing time is estimated to be 35.5 min/blade ($4 \cdot 8.8$) for the second combination of heaters (2 IR-X and 1 Halogen).

6.5.1 Forced wind convection

If the wind and cooling affect is considered into the model to investigate how much it would affect the de-icing time, natural and forced convection according to Section 3.3.1 is included.

If a wind speed of 20 m/s in -15 °C is assumed, the de-icing time would be affected as seen in Figure 67a.

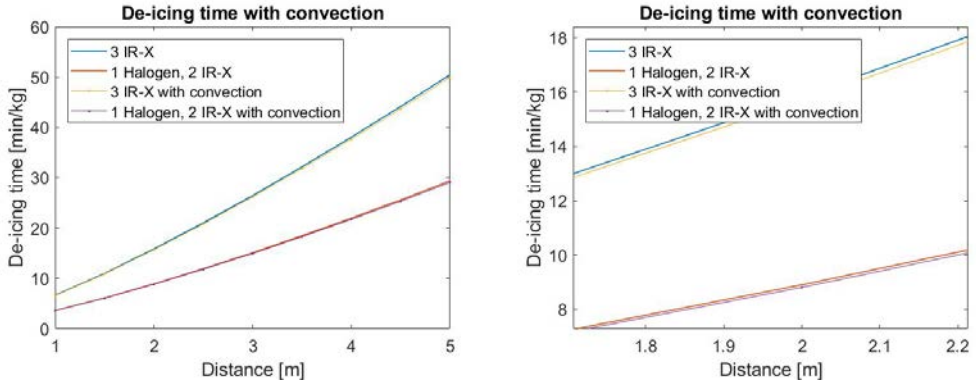

(a) De-icing time with convection.

(b) Zoomed in values.

Figure 67: De-icing time with convection considered for the two combination of heaters.

7 Analysis

In this section analyses are presented for the correlation between the parameters for small scale test and full scale tests.

7.1 Small scale tests, glaze ice

All the tests that were performed had some variations of the parameters that was aimed to keep constant. Because of this, the tests can not be compared only from one parameter.

Some of the results had parameters that differs a lot for the heaters and makes it really hard to compare the results. For an example was the type of de-icing different for the Halogen, where the heater was heating the blade and not melting the ice as for the other heaters. This makes it impossible to compare the power needed to melt ice for an example. Instead all of the parameters have to be considered and weighted against each other to evaluate the most efficient heater for this purpose.

7.1.1 IR-X

Two tests were performed at two different distances with the IR-X heater. The first test at 1 m distance, took a long time and was ended after 2 hours, but the de-icing time was measured as 1 hour and 45 minutes. The test was ended but the plate had a small piece of ice left. The melt water was extracted immediately so only the ice that was melted could be weighted and determined.

The second test was at 0.5 m distance and had a de-icing time of 30 minutes. This clearly shows that the intensity is really important and also confirms the results from the intensity measurements.

Both tests showed clearly that the ice was melted from outside to inside. The melting started immediately after the heater was started. In Figure 42b it shows that this heater was the heater that was heating up the climate chamber the most. This has to be further investigated if it is possible that it is an error.

From the intensity tests and calculation, it indicates that the IR-X has the highest intensity for longer distances.

7.1.2 Carbon

The Carbon heater had results very similar to the IR-X heater. The de-icing was in the same way and melting from the outside of the ice. Many of the properties, as wavelength, temperature and emissivity was very similar for the Carbon and IR-X heater. The Carbon heater had the lowest intensity compared to the other infrared heaters.

Compared to the other tests performed at 0.5 m, Carbon was the heater with farthest de-icing time. This in first hand depends on that the mass of the ice was almost 1 kg more than for the IR-X test. But if the mass of the ice is scaled against the time as kg per minute, the result is almost identical to the results for the IR-X.

7.1.3 Halogen

The results for the halogen heater was very different from the the other heaters. The halogen heater worked in another way than melting the ice. The result of the tests showed that the ice fell of the blade and the temperature of the blade was increasing fast. Because the first test was so deviant from the tests with the other heaters, a second test was done at the same distance. The first ice was placed vertical because the plate was not wide enough to place it the same way as the first tests. This was a factor that was considered to have affected the result. Another reason was due to the fact that there were cracks in the ice and that the ice was not strong enough to attach to the plate from the very beginning. The second test was done in the same way as the other heaters with a horizontal placing and showed the same behavior as for the first test.

The test was very efficient in factors of time. By just watching the test it showed clearly that the radiation was going through the ice and heated the surface of the blade and visible that water was moving behind the ice and water that was dripping as well. This seems reasonable thus the lower wavelength is in theory passing through the ice because of the low albedo. So for the ice melting, this should be a good way to accomplish de-icing. In other hand does snow not act the same way as ice. Snow has a higher albedo and reflects the radiation on the surface of the snow. And as seen in Figure 20 a wavelength longer than about 2 μm is desired.

Other aspects to consider is that the heater had a lot of visible light which can be explained with that it has a lower value for the wavelength peak and

thereby closer to visible light. This can be a problem if it is placed on the tower, approximately 40 meters up in the air. The problem is both for the air force and the community that can be disturbed by the intense light.

If the radiation is heating up the blade and not the ice, the time of radiation acting on the blade can be a problem as well. Heating the blade too much can cause burn marks and erosion that will destroy the blade.

The filament is really hot and heating the cover of the heater as well. Energy that is not used for melting/heating the ice.

7.2 Small scale tests, snow

The small scale tests performed with snow in -15 °C and -30 °C did not show any significant differences. Compared to the glaze ice tests the experiments were only conducted with the Halogen and IR-X heaters. The Carbon heater was excluded due to the similarities with the IR-X noted in the first experiments with glaze ice.

IR-X and Halogen did melt the snow in the same way, for this tests the shorter wavelength could not penetrate the snow like it could for the glaze ice. Although, the start sequence recorded with the thermal camera was about 1 min faster for the Halogen heater than the IR-X, as seen in Table 12, this was also noted visually in the experiments.

The de-icing time for the two temperatures varies, for the IR-X the experiment was faster for -30 °C compared to -15 °C and for the Halogen heater it was the other way around. The variation in time is mostly caused by differing thickness between the snow samples, which was also noted visually. Since it takes more energy to do the phase change, the latent energy, than to heat up the snow to the melting point it is reasonable that variation in time is not that significant between the starting temperatures.

7.3 Full scale tests

Comparing the tests for the large scale experiments is divided into three parts to see how the different parameters differs and affects the efficiency of the melting and de-icing time. All the values for the different tests are presented in Table 13 in Section 6.

7.3.1 Different distances

Performing the tests at different distances gave a significant difference between the results. It is known that the intensity of the radiation decreases with distance and that can be interpreted as "the closer, the better" in the case of de-icing fast. That may be the case, but a limit to not heat the blade to much was set to 40 °C. The energy that is used for de-icing the blade should be focused only to the energy to melt the ice and not heat the blade, which in this case can be assumed to be some type of losses. The results from the performed tests, with our temperature condition, showed that for a closer distance, 1 m in this case, the risk of heating the blade is higher than for the longer distance, 1.5 m.

Comparing Test 2 (1 m) and Test 3 (1.5 m) shows that the melting rate for Test 2 is higher than for Test 3. But comparing the efficiency, which is the quota of the energy needed to de-ice the blade and the energy that is used from the heaters, a higher efficiency is achieved for the longer distance. This is most likely due to the fact of how the the heaters and the reflectors are designed. The radiation is more concentrated to a smaller spot for the shorter distance and more distributed for the longer distance, more about this in Section 6.1.2.

Almost the same results were received from Test 4 and 5 which also gave a higher efficiency for the longer distance (Test 5).

Another interesting value to study is the temperature gradient, which is the slope of how fast the maximal temperature increases after the melting starts, see a more specified definition in Section 5.5. This gives a knowledge of how fast the blade will be heated, and a lower value for the gradient is desired. For both Test 2 - Test 3 and Test 4 - Test 5, the temperature gradient was higher for the shorter distances (Test 2 and Test 4), which means that the shorter distance affects the efficiency negative and that the temperature on the blade increases faster than for the longer distance.

7.3.2 Different combinations of heaters

The two different combinations of heaters also gave results that had a significant difference. Test 3 and Test 5 (3 IR-X, 2 IR-X and 1 Halogen) was performed in the same conditions in terms of distance and snow type. From Table 13 in Section 6 the melting rate and efficiency was higher for the second combination of heaters. The temperature gradient for the second combina-

tion was lower which means that the blade does not heat up as quickly as for the first combination. But the temperature gradient for the first combination was still quite low so the difference was not as significant as for the other values.

From the intensity measurements in Section 6.1.2 the results were very similar. The distribution of the radiation on the surface was also similar but the second combination had a slightly higher power that was radiated on the surface.

7.3.3 Different snow types

The tests with the different types of snow, for the full scale tests with wet and dry snow, did not gave any significant impact of the results. For Test 5 and 6 the efficiency and melting rate was almost identical and the difference between the temperature gradient is negligible.

8 Discussion and Conclusion

Main conclusions for the project:

- The method of having a de-icing system based on infrared radiation works, but not efficient enough.
- Wavelength and distance affects the efficiency.
- Temperature and snow type does not have a significant impact.
- The combination of two different wavelengths gives the fastest and most efficient de-icing on 1.5 m distance.

The first bullet point implies that the method is not efficient enough, and this is compared to commercial and well implemented systems that are used on today's wind turbines. Compared to the system with thermal heat elements and Juktan wind farm, the infrared based system is not competitive in order of de-icing time and required power output. But hence this is only the start of the project it is still possible that this system with some development turns out to be more efficient.

What has been clear from the results of the tests are that the wavelength of the radiation has affected the efficiency and de-icing time. For example, the small scale test with the halogen heater, with shorter wavelength, on glaze ice showed that the radiation was passing through the ice and created a film of water which resulted in the ice fell from the plate. This was different compared to the longer wavelength that melted the ice from outside to inside. But for the small scale tests on a snow surface, it was not any significant difference between the radiation.

If we instead look at the different full scale tests and the different heater combinations, the difference was larger. The combination with the two different wavelengths appeared to be more efficient in form of de-icing time which also was seen in efficiency and melting rate. This is probably due to that the wavelength spectra is wider than just the spectra for heaters with the same wavelength. This could mean that with the wider spectra, the radiation is absorbed better due to the inconsistent snow surface.

The distance of the de-icing has also showed to have an impact of the efficiency. From the intensity measurements and the full scale tests it have showed that a too short distance, as 1 m, endanger that the blade is heating up too much instead of melting the ice evenly on the blade. This is due to the uneven distribution at 1 m distance where the radiation is a lot more

concentrated to the middle. A too long distance will increase the de-icing time significantly and therefor not be as sufficiently effective.

The difference between the snow types was negligible. The efficiency and melting rate for the two compared tests in Section 6.4 were almost the same and there was no visible difference between the tests. The non-existent difference is mostly due to the very similar snow types that were used. It was very hard to decide specific snow conditions and to create a very specific type of snow with the snow machines. Therefor it is hard to have any real conclusions about the snow type when the most of the characteristics are unknown.

The small scale tests performed in different temperatures did not have any significant results that differed. The only thing that was different was the "start-up sequence", the time for the surface to reach 0 °C. In the colder temperatures the start-up sequence was a bit longer but nothing that had an impact of the total de-icing time in the end. This is correlated to the theory where the energy to heat the snow to 0 °C from the starting temperature is so much lower than the energy that is required to melt the ice, for the phase change.

The most efficient test was the test with the heater combination with combined wavelengths performed at a distance that was 1.5 m.

8.1 Uncertainties and errors

The small scale tests with performed with the glaze ice was performed in a climate chamber at LTU. The chamber was small and when the tests were performed the heater affected the surrounding temperature a lot. This can also be seen in the temperature graphs in Section 6.2. This may have affected the de-icing time and the de-icing sequence. For one of the tests, the chamber started a de-frosting sequence which increased the temperature in the chamber even more.

When the glaze ice was created and the boxes was released from the surface, there were cracks formed in the ice. In some of the cases pieces came loose from the plate and had to be "glued" back to the plates. This may also have affected the de-icing.

Because the Halogen heater made the ice to drop from the plates, the energy used to melt the ice can not be compared in the same way as for the heaters that melted the ice from the outside.

The model that is used to estimate the de-icing time for the different heater combinations and distances is depending on the efficiency from the tests that were performed. The efficiency is calculated as an average from all the tests and the distance is not taken into account.

The total radiated power was calculated from the 9 points that was measured for the intensity tests. It is possible that there were too few points measured to be certain that the power and distribution of the radiation is accurate. But it gives a good estimation of the relation between power and distance.

For Test 7 and 8, the NI-DAQ was re-calibrated due to the tests performed in the climate chamber in -30 °C. This gave errors in the load cell and the measurements of the weight. These errors was also included in the efficiency and therefor also the model that was created.

During the full scale tests there was snow that fell from the ceiling onto the blade during the performed test which may have affected the weight measurements a bit, mostly before the melting started.

9 Further Work

First of all, the infrared heaters needs to be rebuilt with a more concentrated beam of radiation and even distribution to cover the whole blade without overheating the surface. The heaters used in this project were built to cover a larger area than the width of a wind turbine blade. When the reflectors are more concentrated, different filaments could be tried out to avoid a high amount of visible light but still have a wide spectra of wavelengths.

With a new design of the heaters some of the experiments from this project could be repeated to determine if there are any improvements. To validate the system even more, field tests can be performed where the cooling of the blade surface caused by the wind is of interest.

In order to achieve a totally de-iced blade on both sides the placing at the tower and the mechanical design needs to be adjusted based on the possibilities to pitch the blade. A deeper investigation needs to be done to develop the mechanics and electronics together with a control system for ice-detection. Interesting would also be if this new de-icing system could be combined with a blade coating that attracts infrared radiation.

The environmental affects caused by the light from the heaters are of importance. As seen in the experiments, the heaters, especially the Halogen, contains a lot of visible light that can disturb animals, people living close by and air crafts. Today there are regulations for how much light that is needed as an obstruction light, but there are no regulations for the maximum amount of light placed on top of a wind turbine.

Resume of the recommendations for future work:

- Design heaters that is suitable for the purpose.
- Investigate the possibilities to pitch the blade.
- Mechanical and electrical design together with a control system.
- Field tests with real weather conditions.
- Impact of the surroundings for an infrared de-icing method.
- Combine the method with a blade coating that attracts infrared radiation.
- Economic viability.

References

1. Wind, I. E. A. *Wind energy in Sweden* Downloaded: 2019-03-27. https://community.ieawind.org/about/member-activities/sweden.
2. Birol, D. F. *Renewables 2018* Downloaded: 2019-03-27. https://www.iea.org/renewables2018/.
3. Agency, T. S. E. Energy in Sweden 2018 (2018).
4. Vattenfall. *Pågående vindkraftprojekt* 2018. Downloaded: 2019-03-01. https://corporate.vattenfall.se/om-oss/var-verksamhet/var-elproduktion/vindkraft/pagaende-vindkraftprojekt/.
5. Chehouri, A. & Hamel, M. Icing Losses - Comparison Between Mast and Turbine Production Data. doi:10.13140/RG.2.2.36636.39046 (Sept. 2017).
6. Malmsten, J. K. Wind Turbine Production losses in Cold Climate (2011).
7. Safanah Mudheher Raafat, R. H. *Power Maximization and Control of Variable-Speed Wind Turbine System Using Extremum Seeking - Scientific Figure on ResearchGate* Downloaded: 2019-04-09. https://www.researchgate.net/figure/Wind-turbine-components-1_fig1_322761950.
8. E.Hau. *Wind turbines - Fundamentals, Technologies, Application, Economics* (Springer Heidelberg New York Dordrecht London, Munich, Germany, 2000).
9. O. Fakorede Z. Feger, H. I.A.I.J.P.C. M. Ice protection systems for wind turbines in cold climate: characteristics, comparisons and analysis. *Renewable and Sustainable Energy Reviews 65 (2016) 662–675.* DOI: 10.1016/j.rser.2016.06.080 (2016).
10. Forsgren, I. O & M Manager, Vattenfall Wind. Interview. 2019-02-05.
11. Froese, M. *Cracking the icing problem on turbine blades* Downloaded: 2019-04-03. https://www.windpowerengineering.com/business-news-projects/cracking-icing-problem-turbine-blades/.
12. Vattenfall. *Stor-Rotliden vindkraftpark* 2017, Downloaded: 2019-03-27. https://corporate.vattenfall.se/om-oss/var-verksamhet/var-elproduktion/vindkraft/stor-rotliden-vindkraftpark/.
13. Vattenfall. *Juktan vindkraftpark* 2016, Downloaded: 2019-03-27. https://corporate.vattenfall.se/om-oss/var-verksamhet/var-elproduktion/vindkraft/juktan-vindkraftpark/.
14. O.Parent, A. *Anti-icing and de-icing techniques for wind turbines: Critical review* 2010. Downloaded: 2019-02-22. https://www.sciencedirect.com/science/article/pii/S0165232X10000108.

15. Laboratory, L. L. N. *Prediciting Wind Power with Greater Accuracy* Downloaded: 2019-05-18. https://str.llnl.gov/april-2014/miller.
16. Suke, P. *Analysis of heating systems to mitigate ice accretion on wind turbine blades* MA thesis (McMaster University, January 2014).
17. Blade-Solutions. *Blade Heat Inspection - Large Hot Spots* Downloaded: 2019-01-21. http://www.bladesolutions.se/.
18. Suke, P. *Analysis of heating systems to mitigate ice accretion on wind turbine blades* MA thesis (McMaster University, January 2014).
19. Borealis-Wind. *De-icing Process* 2017. Downloaded: Feb. 2019. https://www.borealiswind.com/.
20. Vestas-Wind-Systems-A/S. *Cold Climate Solutions* 2018. Downloaded: Feb. 2019. http://nozebra.ipapercms.dk/Vestas/Communication/Productbrochure/TurbineOptions/VestasColdClimateSolutions/?page=2.
21. ENERCON. *ENERCON Magazine for wind turbine* Downloaded: 2019-03-04. https://www.enercon.de/fileadmin/Redakteur/Medien-Portal/windblatt/pdf/en/wb_01-2011_en.pdf.
22. Communitech. *We Built This — Borealis Wind* Apr. 19 2017. Watched: Feb. 2019. https://www.youtube.com/watch?v=V4yxFxmcCyY.
23. Skybrary. *Ice formation on aircraft* Downloaded: 2019-03-26. https://www.skybrary.aero/index.php/Ice_Formation_on_Aircraft.
24. Rosenlof, K. *Infrared De-icing Speeds Process and Reduces Cost* 2013. Downloaded: 2019-02-27. https://www.ainonline.com/aviation-news/aviation-international-news/2013-10-02/infrared-de-icing-speeds-process-and-reduces-cost.
25. ELCOM. *Far-infrared Snow-melting device* 2016. Downloaded: 2019-02-25. http://www.elcom-jp.com/english/products/tokermo/tokermo.html.
26. EC-Online. *Mul-T-Mount Electric Infrared Heater* Downloaded: 2019-02-25. https://www.econline.com/doc/mul-t-mount-electric-infrared-heater-0001.
27. Lightening-Specialties. *Infrared Electric Heaters - General Product Information* Downloaded: 2019-03-01. https://catalog.lightingspecialties.com/Asset/Fostoria-Mul-T-Mount.pdf.
28. S.Fikke G.Ronsten, S.-M.P.J.B.B.J.T.K. L. COST 727: Atmospheric Icing on Structures Measurements and data collection on Icing: State of the Art. *Veröffentlichung MeteoSchweiz.* ISSN: 1422-1381 (2006).
29. Nationalencyklopedin. *Adhesion* Downloaded: 2019-04-10. http://www.ne.se.proxy.lib.ltu.se/uppslagsverk/encyklopedi/lÃěng/adhesion-(fysik).

30. Nationalencyklopedin. *Kohesion* Downloaded: 2019-04-10. http://www.ne.se.proxy.lib.ltu.se/uppslagsverk/encyklopedi/lÃěng/kohesion.
31. Unknown. *Soft Rime Ice, Picture* Downloaded: 2019-02-27. https://upload.wikimedia.org/wikipedia/commons/f/fc/Raureif2.JPG.
32. Unknown. *Hard Rime Ice, Picture* Downloaded: 2019-02-27. https://createarcticscience.files.wordpress.com/2014/07/img_1301.jpg.
33. Unknown. *Glaze Ice, Picture* Downloaded: 2019-02-27. https://upload.wikimedia.org/wikipedia/commons/0/0c/Freezing_Rain_on_Tree_Branch.jpg.
34. Rouse, M. *Infrared radiation* 2017, Downloaded: 2019-03-27. https://searchnetworking.techtarget.com/definition/infrared-radiation.
35. Optex. *Electromagnetic spectra for infrared radiation* Downloaded: 2019-05-24. http://www.optex.net/global/tech/infrared.html.
36. Huete, A. *Remote sensing for environmental monitoring* Downloaded: 2019-04-10. https://www.sciencedirect.com/science/article/pii/B9780120644773500138.
37. Toolbox, T. E. *Convective Heat transfer* Downloaded: 2019-06-03. https://www.engineeringtoolbox.com/convective-heat-transfer-d_430.html.
38. Frico. *Carbon or halogen – which infrared heater is best?* Downloaded: 2019-05-18. http://www.frico.se/en/Our-knowledge/Articles/Comfort/carbon-or-halogen--which-infrared-heater-is-best/.
39. Opranic. *Theory of infrared heating* Downloaded: 2019-02-28. https://opranic.com/infrared-heating/.
40. Kanthal. *Thermopiles* Downloaded: 2019-03-21. https://www.kanthal.com/en/applications/thermopiles/.
41. Rousk, M. Technical salesmen, Norveco. E-mail. 2019-03-03.
42. testo. *testo 875i, Thermal imager. Instruction manual* Downloaded: 2019-03-21. https://www.testo.com/en-US/testo-875i-1/p/0563-0875-V1.
43. Nordtec-Instrument. *Kortfattad termografi - fakta* Downloaded: 2019-03-21. https://nordtec.se/fakta-matteknik/termografi.
44. Pentronic. *Termoelementtråd PVC-isolerad Modell P-24* Downloaded: 2019-04-17. https://pentronic.se/start/temperaturgivare/kablar-och-kontakter/termoelementtraad.aspx?navigateto=true&article=04-20230.
45. Veteke. *S-Lastcell för tryck och drag 300 kg. IP67. Nickelpläterat stål.* 2019, Downloaded: 2019-03-27. https://www.vetek.se/s-lastcell-

for-tryck-och-drag-300-kg-ip67-nickelplaterat-stal-vz101-bh-300kg-sv/article.

46. Veteke. *Datasheet 101BH.* 2010, Downloaded: 2019-03-27. https://www.vetek.se/Dynamics/Documents/a80e20e2-25b6-4bd4-85c8-716baf560ad7/Datasheet%20101B.pdf.
47. Tacunasystems. *The essential guide to load cells.* Downloaded: 2019-03-27. https://tacunasystems.com/knowledge-base/load-cell-tips/the-essential-guide-to-load-cells/.
48. HMB. *Measuring with strain gauges: How to prevent unwanted temperature effects on your measurement result* Downloaded: 2019-03-27. https://www.hbm.com/en/6725/article-temperature-compensation-of-strain-gauges/.
49. National-Instrument. *NI 9219 Getting Started Guide* Downloaded: 2019-03-21. http://www.ni.com/pdf/manuals/374473f.pdf.
50. Tech, J. D. *Background of Thermopiles* Downloaded: 2019-03-21. https://www.jondetech.se/technology/background-of-thermopiles/.
51. Ophir. *Low Power Thermal Sensors* Downloaded: 2019-03-21. https://www.ophiropt.com/laser--measurement/sites/default/files/10A_30A-BB-18_L30A-10MM_L30A-EX-10MM_50%28150%29A-BB-26.pdf.

Appendix A - Case Study: Stor-Rotliden

Stor-Rotliden is one of Vattenfall AB:s wind parks located 20 kilometer from Frederika, Västerbotten. With 40 turbines of the model Vestas V90 and installed power of 78 MW, it is Vattenfalls largest landbased park. Expected yearly production is about 240 GWh and has no de-icing or anti-icing system installed. Operational conditions is set to temperature limits of -20 to +30 °C which means they only operates between these temperatures.

Losses

Even though the wind park is located in a location with a large risk of cold climate, it has no de-icing system. This affects the production more than expected. The losses due to operation in cold climate can be divided into two types of losses:

- Standstill losses,
- Performance losses.

Standstill losses is the loss of power when standing still because of ice and snow. The conditions for this is that the *Active Power* is less than 0 kWh and the *Ambient Temperature* is less than 0 °C. The conditions for Performance losses is when the *Active Power* is less than 80 % of the Expected Power, which is the power "promised" from the manufacturer at current wind speed, see Figure 68.

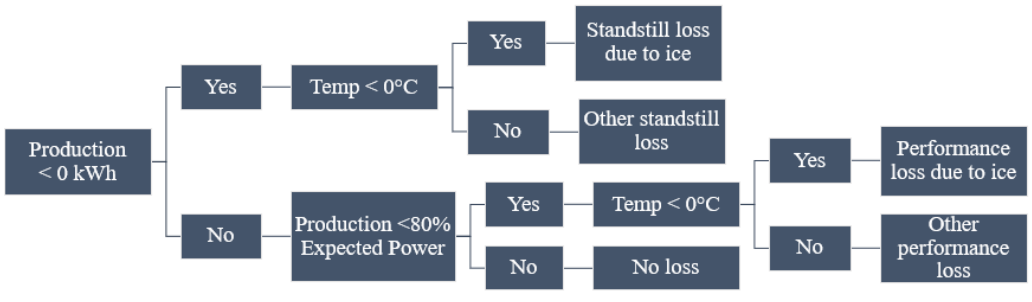

Figure 68: Flowchart of how to determine the losses.

From logged data collected from *"Windwebportal"*, an internal software at

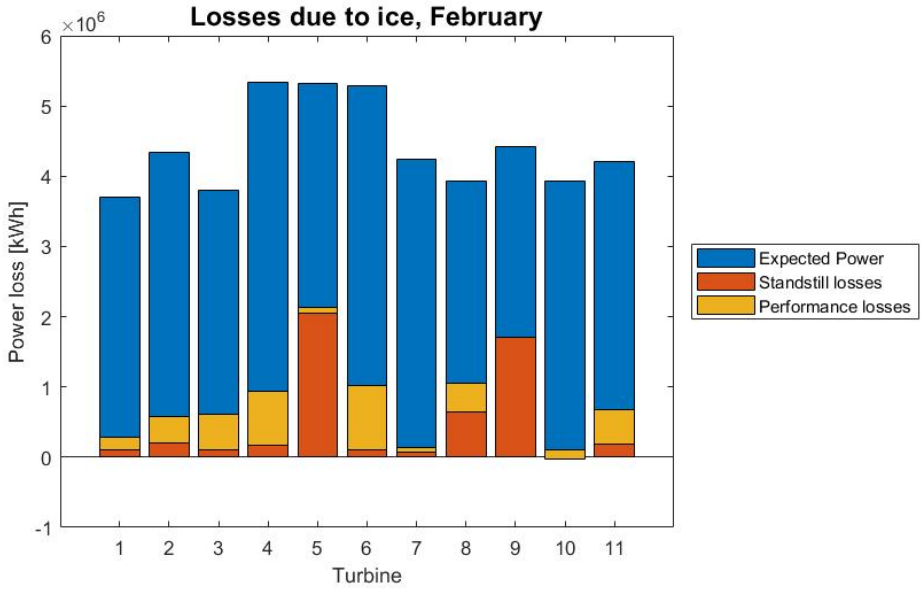

Figure 69: Bar graph for the distribution of losses and the expected power.

Vattenfall, losses from February 2018 has been determined. For the first 11 turbines in Stor-Rotliden the losses and expected power is shown as in Figure 69.

Appendix B - Thermal tables

Table 14: Prandtl number.

Temperature [°C]	Prandtl number
213.2	4.138
-193.2	1.7
-173.2	0.78
-153.2	0.759
-133.2	0.747
-93.2	0.731
-73.2	0.726
-53.2	0.721
-33.2	0.717
-13.2	0.713
0	0.711
6.9	0.71
15.6	0.709
26.9	0.707
46.9	0.705
66.9	0.703
86.9	0.701
106.9	0.7
126.9	0.699
226.9	0.698
326.9	0.703
426.9	0.71
526.9	0.717
626.9	0.724
726.9	0.73
826.9	0.734

Appendix C - List of equipment

List of all equipment used for the experiments:

- Infrared heaters
- Frame for the infrared heaters
- Section of a wind turbine blade
- Stand for the blade section
- Test plates in glass fiber
- Thermal camera and charger
- Stand for thermal camera
- Thermocouples
- Load cell
- NI-DAQ 9219
- Thermopile sensor
- Computer and notebook
- Three wire cable
- Distribution board
- Residual current device
- Water sprayer
- Snow cannon
- Fan
- Camera
- Power bank
- Measuring tape
- Table
- Weather station
- Ladder
- Snow shovel
- Stopwatch
- Plastic bags
- Gloves
- Safety glasses
- Extinguishers
- Warm clothes and shoes

Appendix D - MATLAB commands

- *findchangepts*, find abrupt changes in a signal
- *imagesc*, displays images with scaled colors
- *rms*, calculates the rot-mean-square value
- *mean*, calculates the mean value
- *spline*, spline interpolation
- *polyval*, finds coefficients to polynomial curve
- *polyfit*, polynomial fit from coefficients

Appendix E - Load cell data sheet

101BH

VETEK

Alloy Steel

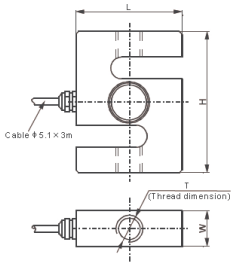

CE Ex RoHS

S-BEAMS

DIMENSIONS

RATED CAPACITY	H	L	W	T
kg/mm				
50···200	76.2	50.8	19.0	M12X1.75
300···1,500; SE2,000**	76.2	50.8	28.2	M12X1.75
2,000···5,000	108.0	76.2	25.4	M18X1.50
10,000	177.8	125.0	50.8	M30X2.00
lb/inches (conversion of above dimensions)				
110.23···440.92	3.00	2.00	0.75	M12X1.75
661.39···3,306.9; SE4,409.2**	3.00	2.00	1.11	M12X1.75
4,409.2···11,023.1	4.25	3.00	1.00	M18X1.50
22,046.2	7.00	4.92	2.00	M30X2.00

SPECIFICATIONS

Rated Capacity	kg	50; 100; 200	300; 500; 1t; SE2t	2t; 3t; 5t	10t
Weight (G), approx.	kg/lb	0.6 / 1.2	0.8 / 1.7	1.4 / 3.1	7.4 / 16.3
Full Scale Output	mV/V	2.0 ± 1%			
Zero Balance	mV/V	±0.04			
Non-linearity	%	< ±0.017			
Repeatability	%	< ±0.017			
Hysteresis Error	%	< ±0.017			
Creep in 30 min.	%	< ±0.023			
Bridge Resistance	Ω	400 ± 25			
Rated Excitation	V(DC/AC)	10 (15V Maximum)			
Insulation Resistance	GΩ	>2 [50 VDC]			
Nominal Temperature Range	°C/°F	-10 to 40 / 14 to 104			
Safe Overload	% of full scale	200			
Breaking Overload	% of full scale	300			
Seal Type		Environmentally-sealed, IP66/IP67			

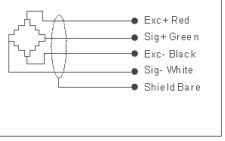

AVAILABLE OPTIONS

- Service temperature range up to 120°C [248°F]
- 6-wire circuit
- Stainless Steel 101BSGS

INTERCHANGEABLE PRODUCTS

Manufacturer	Model
Vishay Tedea-Huntleigh	615
Vishay Tedea-Huntleigh	616

www.vetek.com

Appendix F - Risk assessment

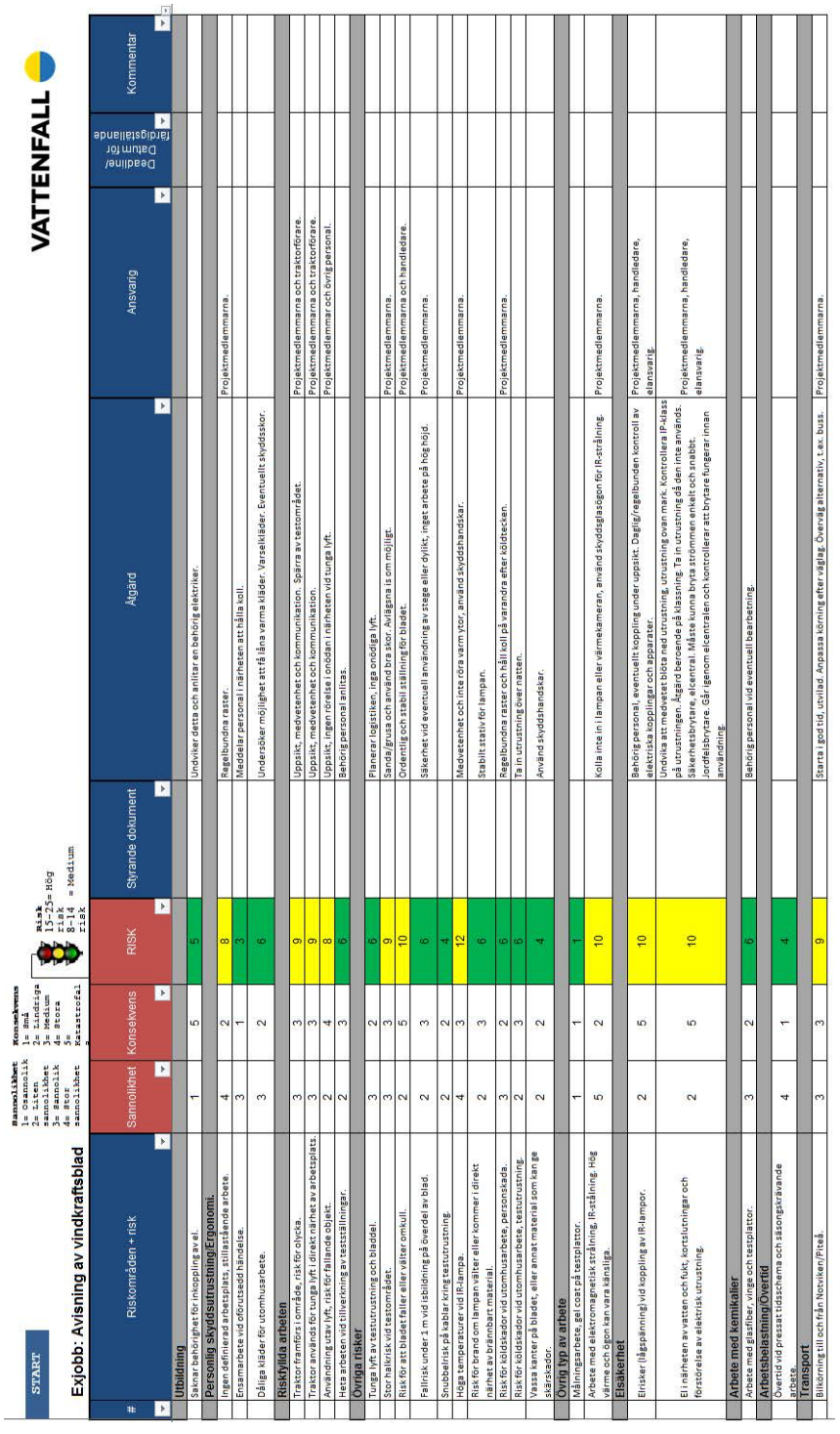

START

Exjobb: Avisning av vindkraftsblad

VATTENFALL

Sannolikhet: 1= Osannolik, 2= Liten sannolikhet, 3= Medium sannolikhet, 4= Stor sannolikhet, 5= Katastrofal

Konsekvens: 1= Små, 2= Lindriga, 3= Medium, 4= Stora, 5= Katastrofala

Risk: 15–25= Hög risk, 8–14 = Medium risk

#	Riskområden + risk	Sannolikhet	Konsekvens	RISK	Styrande dokument	Åtgärd	Ansvarig	Deadline/ Datum för färdigställande	Kommentar
	Utbildning								
	Saknar behörighet för inkoppling av el.	1	5	5		Undviker detta och anlitar en behörig elektriker.			
	Personlig skyddsutrustning/Ergonomi.								
	Ingen definierad arbetsplats, stillastående arbete.	4	2	8		Regelbundna raster.	Projektmedlemmarna.		
	Ensamarbete vid oförutsedd händelse.	3	1	3		Meddelar personal i närheten att hålla koll.			
	Dåliga kläder för utomhusarbete.	3	2	6		Undersöker möjlighet att få låna varma kläder/ Varselkläder. Eventuellt skyddsskor.			
	Risktyida arbeten								
	Traktor framförs i område, risk för olycka.	3	3	9		Uppsikt, medvetenhet och kommunikation. Spärra av testområdet.	Projektmedlemmarna och traktorförare.		
	Traktor används för tunga lyft i direkt närhet av arbetsplats	3	3	9		Uppsikt, medvetenhet och kommunikation.	Projektmedlemmarna och traktorförare.		
	Användning utav lyft, risk för fallande objekt	2	4	8		Uppsikt, ingen närvaro i området i närheten vid tunga lyft.	Projektmedlemmar och övrig personal.		
	Heta arbeten vid tillverkning av teststållningar.	2	3	6		Behörig personal anlitas.			
	Övriga risker								
	Tunga lyft av testutrustning och bladdel.	3	2	6		Planerar logistiken, inga onödiga lyft.			
	Stor halkrisk vid testområdet.	3	3	9		Sanda/grusa och använd bra skor. Avlägsna is om möjligt.	Projektmedlemmarna.		
	Risk för att bladet faller eller välter omkull.	2	5	10		Ordentlig och stabil ställning för bladet.	Projektmedlemmarna och handledare.		
	Fallrisk under 1 m vid isbildning på överdel av blad.	2	3	6		Säkerhet vid eventuell användning av stege eller dylikt, inget arbete på hög höjd.	Projektmedlemmarna.		
	Snubbelrisk på kablar kring testutrustning.	2	2	4					
	Höga temperaturer vid IR-lampa.	4	3	12		Medvetenhet och inte röra varm ytor, använd skyddshandskar.	Projektmedlemmarna.		
	Risk för brand om lampan välter eller kommer i direkt närhet av brännbart material.	2	3	6		Stabilt stativ för lampan.			
	Risk för köldskador vid utomhusarbete, personskada.	3	2	6		Regelbundna raster och håll koll på varandra efter köldtecken.	Projektmedlemmarna.		
	Risk för köldskador vid utomhusarbete, testutrustning.	2	3	6		Ta in utrustning över nästen.			
	Vassa kanter på bladet, eller annat material som kan ge skärsår.	2	2	4		Använd skyddshandskar.			
	Övrig typ av arbete								
	Mätningsarbete, gel coat på testplattor.	1	1	1					
	Arbete med elektromagnetisk strålning, IR-strålning. Hög värme och ögon kan vara känsliga.	5	2	10		Kolla inte in i lampan eller värmekameran, använd skyddsglasögon för IR-strålning.	Projektmedlemmarna.		
	Elsäkerhet								
	Elrisker lågspänning vid koppling av IR-lampor.	2	5	10		Behörig personal, eventuellt koppling under uppsikt. Daglig/regelbunden kontroll av elektriska kopplingar och apparater.	Projektmedlemmarna, handledare, elansvarig.		
	Eli närheten av vatten och fukt, kortslutningar och förstörelse av elektrisk utrustning.	2	5	10		Undvika att medvetet blöta ned utrustning, utrustning ovan mark. Kontrollera IP-klass på utrustningen. Åtgärd beroende på klassning. Ta in utrustning då den inte används. Säkerhetsbrytare, elcentral. Måste kunna bryta strömmen enkelt och snabbt. Jordfelsbrytare. Går igenom elcentralen och kontrollerar att brytare fungerar innan användning.	Projektmedlemmarna, handledare, elansvarig.		
	Arbete med kemikalier								
	Arbete med glasfiber, vinge och testplattor.	3	2	6		Behörig personal vid eventuell bearbetning.			
	Arbetsbelastning/Överlid								
	Överlid vid pressat tidsschema och säsongsrävande arbete.	4	1	4					
	Transport								
	Bilkörning till och från Nordviken/Piteå	3	3	9		Starta i god tid, utvilad. Anpassa körning efter vägtag. Överväg alternativ, t.ex. buss.	Projektmedlemmarna.		

Appendix G - Small scale results

Test A: IR-X 1 m, glaze ice

(a) Image, start.

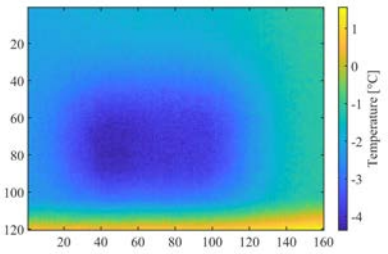

(b) Heat chart, start.

(c) Image, 5 min.

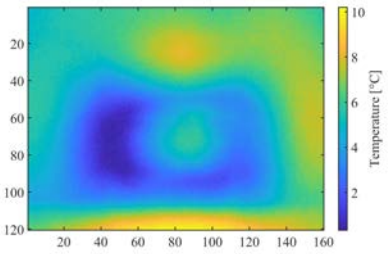

(d) Heat chart, 5 min.

(e) Image, 20 min.

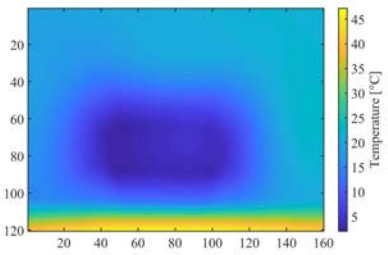

(f) Heat chart, 20 min.

(g) Image, 75 min.

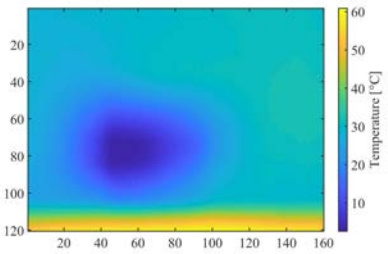

(h) Heat chart, 75 min.

Figure 70: Images and heat charts for Test A, IR-X 1 m, glaze ice.

Test C: Halogen 0.5 m, glaze ice, first

(a) Image, start.

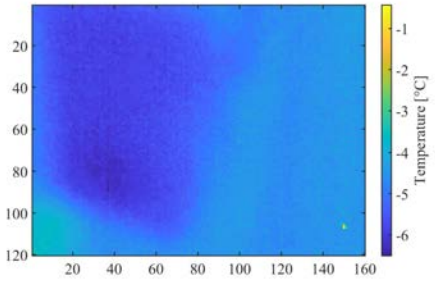

(b) Heat chart, start.

(c) Image, 5 min.

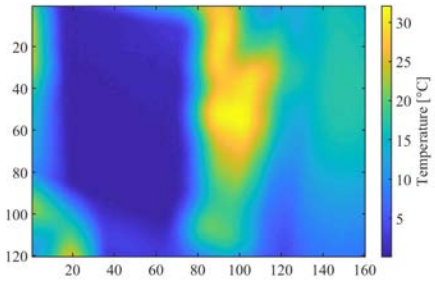

(d) Heat chart, 5 min.

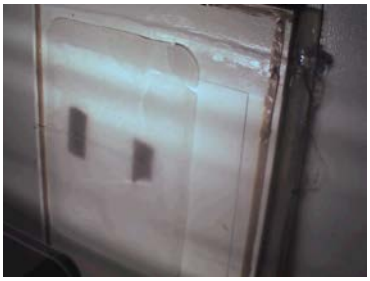

(e) Image, 20 min.

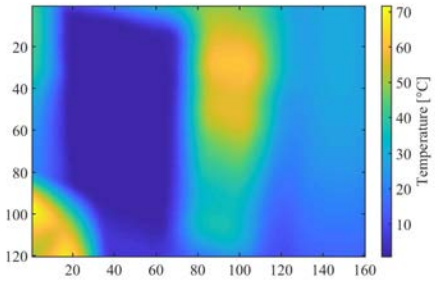

(f) Heat chart, 20 min.

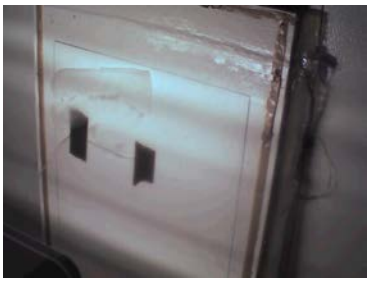

(g) Image, 25 min.

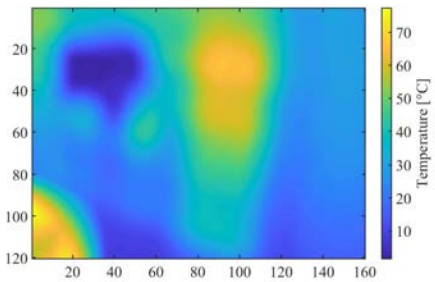

(h) Heat chart, 25 min.

Figure 71: Images and heat charts for Test C, Halogen 0.5 m, glaze ice.

Test D: Carbon 0.5 m, glaze ice

(a) Image, start.

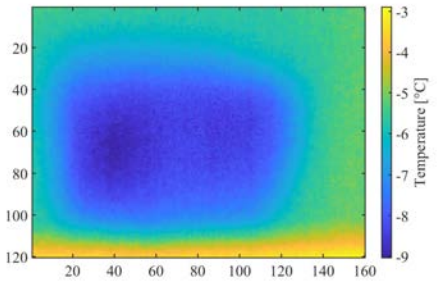

(b) Heat chart, start.

(c) Image, 5 min.

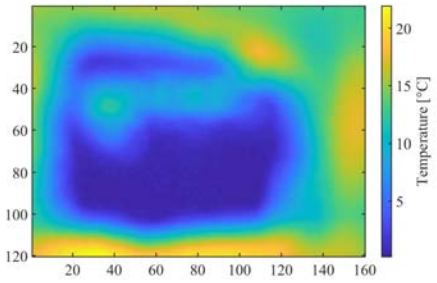

(d) Heat chart, 5 min.

(e) Image, 20 min.

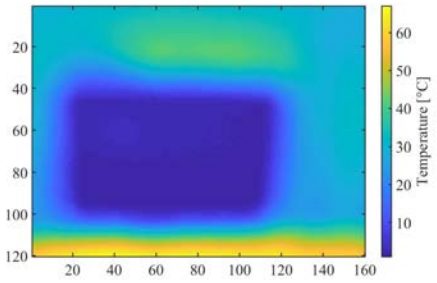

(f) Heat chart, 20 min.

(g) Image, 45 min.

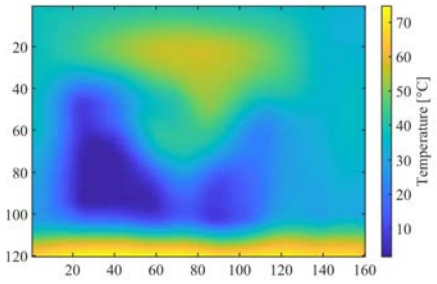

(h) Heat chart, 45 min.

Figure 72: Images and heat charts for Test D, Carbon 0.5 m, glaze ice.

Appendix H - Full scale results

Test 1: 3 IR-X at 1 m, dry snow

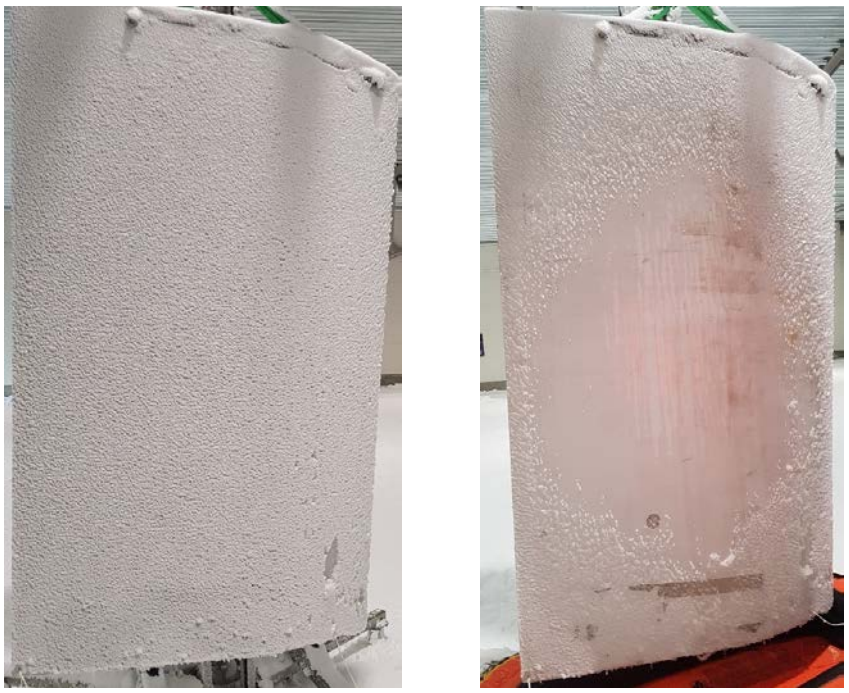

(a) Surface of blade before de-icing. (b) Surface after de-iced blade.

Figure 73: Images of full blade for Test 1.

(a) Trailing edge. (b) Leading edge.

Figure 74: Images of snow on the edges for Test 1.

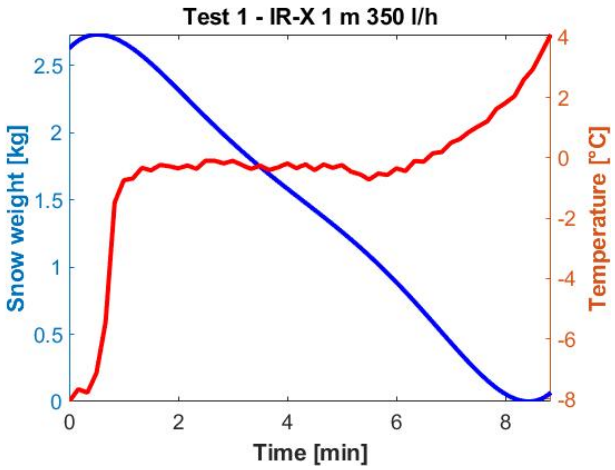

Figure 75: Weight and temperature graph for Test 1.

Test 7: 3 IR-X at 1.5 m, wet snow

(a) Surface of blade before de-icing. (b) Surface after de-iced blade.

Figure 76: Images of full blade for Test 7.

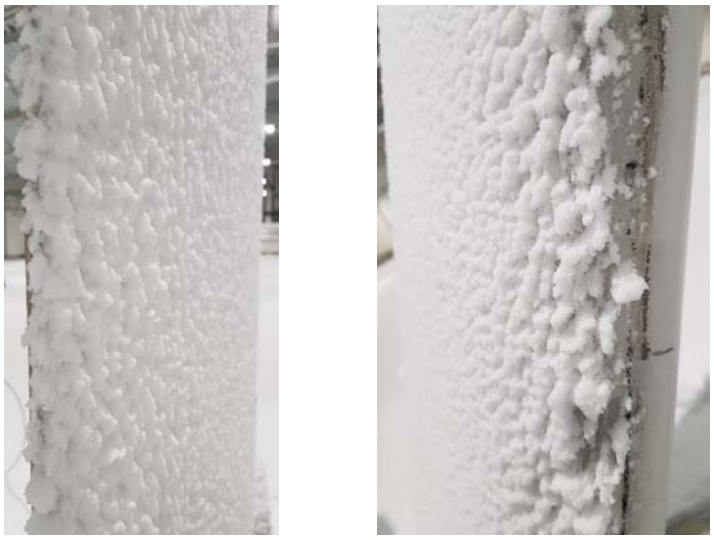

(a) Trailing edge. (b) Leading edge.

Figure 77: Images of snow on the edges for Test 7.

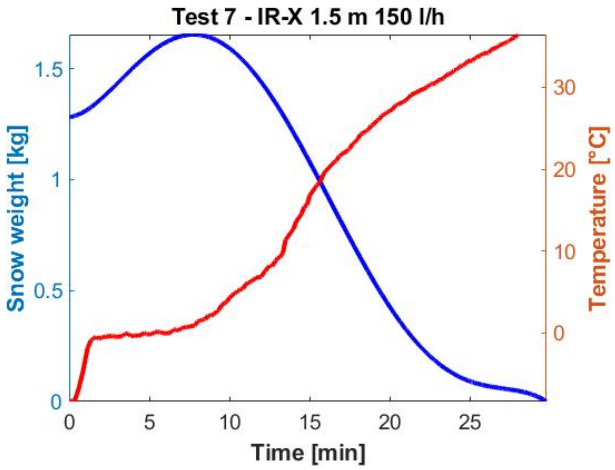

Figure 78: Weight and temperature graph for test 7.

Test 8: 3 IR-X at 1.5 m, wet snow

(a) Surface of blade before de-icing. (b) Surface after de-iced blade.

Figure 79: Images of full blade for Test 8.

(a) Trailing edge. (b) Leading edge.

Figure 80: Images of snow on the edges for Test 8.

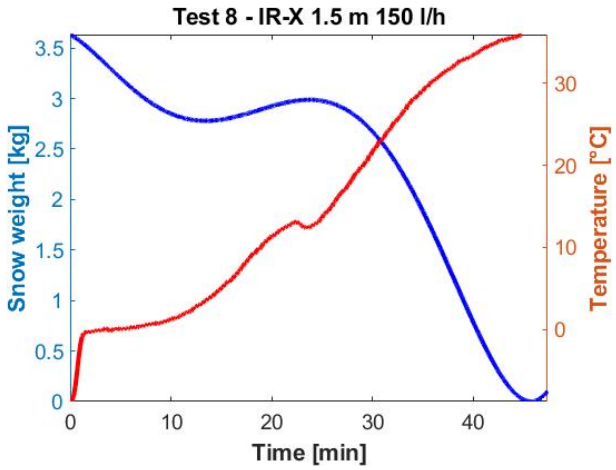

Figure 81: Weight and temperature graph for Test 8.